

TRANSPORT OF EMERGING CONTAMINANTS IN POROUS MEDIA

by

Yake Wang

Copyright © Yake Wang 2019

A Dissertation Submitted to the Faculty of the

DEPARTMENT OF ENVIRONMENTAL SCIENCE

In Partial Fulfillment of the Requirements

For the Degree of

DOCTOR OF PHILOSOPHY
WITH A MAJOR IN ENVIRONMENTAL SCIENCE


In the Graduate College

THE UNIVERSITY OF ARIZONA

2019

THE UNIVERSITY OF ARIZONA
GRADUATE COLLEGE

As members of the Dissertation Committee, we certify that we have read the dissertation prepared by Yake Wang, titled Transport of Emerging Contaminants in Porous Media and recommend that it be accepted as fulfilling the dissertation requirement for the Degree of Doctor of Philosophy.


Date: 8/14/2019
Mark Brusseau



Date: 8/14/2019
Janick Artola


Date: 8/14/2019
Mónica Ramírez-Andreotta


Date: 8/14/2019
Juliana Araujo

Final approval and acceptance of this dissertation is contingent upon the candidate's submission of the final copies of the dissertation to the Graduate College.

I hereby certify that I have read this dissertation prepared under my direction and recommend that it be accepted as fulfilling the dissertation requirement.


Date: 8/14/2019
Dissertation Director: Mark Brusseau

ACKNOWLEDGEMENTS

I would like to thank my advisor, Dr. Mark Brusseau for his guidance and help. I would also like to thank my committee members Drs. Janick Artiola, Mónica Ramírez-Andreotta and Juliana Araujo, and members of the Contaminant Transport Lab for their help. Finally, I want to thank my mom, dad and brother for their support.

TABLE OF CONTENTS

LIST OF TABLES AND FIGURES.....	6
ABSTRACT.....	7
CHAPTER 1. INTRODUCTION.....	8
1.1 Transport of Graphene and Graphene Oxide in Saturated Porous Media	8
1.1.1 Research Purpose.....	8
1.1.2 Literature Review.....	9
Graphene and Graphene Oxide Nanoparticles.....	9
Surfactant-dispersed Graphene Suspension.....	10
Colloid Filtration Theory	12
1.2 Nonideal Transport and Extended Elution Tailing of PFOS in Soil and Aquifer Sediment	14
1.2.1 Research Purpose.....	14
1.2.2 Literature Review.....	15
PFASs	15
Two-domain Sorption-kinetics (TDSK) Model.....	18
Continuous-distribution Multi-rate (CDMR) Model	20
FIGURES.....	22
CHAPTER 2. PRESENT STUDY.....	26
2.1 Transport of Graphene and Graphene Oxide in Saturated Porous Media	26
2.1.1 Materials and Methods.....	26
2.1.2 Summary of the Results.....	27
2.2 Nonideal Transport and Extended Elution Tailing of PFOS in Soil and Aquifer Sediment	29
2.2.1 Materials and Methods.....	29
2.2.2 Summary of the Results.....	30
2.3 Conclusions.....	36
REFERENCES	39
APPENDIX A – TRANSPORT OF GRAPHENE AND GRAPHENE OXIDE IN SATURATED POROUS MEDIA.....	49
Abstract.....	50
1. Introduction.....	51
2. Materials and Methods.....	52
2.1 Materials	52

2.2. Preparation of Suspensions	53
2.3. Column Experiments	54
2.4. Data Analysis	54
3. Results and Discussion	56
4. Conclusion	62
Acknowledgements.....	63
References.....	63
APPENDIX B – NONIDEAL TRANSPORT AND EXTENDED ELUTION TAILING OF PFOS IN SOIL AND AQUIFER SEDIMENT.....	75
Abstract	76
1. Introduction.....	77
2. Materials and Methods.....	78
2.1 Materials	78
2.2 Miscible-displacement Experiments.....	79
2.3 Analytical Methods.....	80
2.4 Simulation for the Experimental Data	81
3. Results and Discussion	83
4. Conclusion	86
Acknowledgements.....	87
References.....	88

LIST OF TABLES AND FIGURES

Figure 1.1. Graphene (top) as a building material for other carbon materials such a 0-dimensional fullerene (bottom left), 1-dimensional carbon nanotube (bottom middle), and 3-dimensional graphite (bottom right). (Geim and Novoselov, 2007).	22
<hr style="border: 0.5px solid black;"/>	
Figure 1.2. Molecular formulas of an anionic surfactant, SDBS (left) and a nonionic surfactant, Tween 80 (right).....	23
Figure 1.3. Three typical micelle formations: (A) spherical, (B) cylindrical, and (C) bilayer (Lugo, 2010).	24
Figure 1.4. Molecular formulas for PFOS (top) and PFOA (bottom).	25
Table 2.1. Properties of the Porous Media.....	32
Figure 2.2. Measured and simulated breakthrough curves for transport of the nonreactive tracer (NRT) and PFOS in Vinton soil (Experiments 1a and 1b). The PFOS simulation is produced using a two-domain model that accounts for nonlinear, rate-limited sorption/desorption (expt 1a: $\beta = 0.39$, $\omega = 0.5$; expt 1b: $\beta = 0.46$, $\omega = 0.74$).....	33
Figure 2.3. Measured and simulated breakthrough curves for transport of PFOS in Vinton soil (Experiment 2). The PFOS simulations are produced using the two-domain sorption-kinetics model (TD) and the continuous-distribution multi-rate model (CD).	34
Figure 2.4. Measured elution waves for transport of PFOS, two HOCs, and a non-reactive tracer (NRT) in Eustis soil. The pore volumes are normalized by dividing by the respective retardation factors (NRT = 1, PFOS = 4.2, atrazine = 3.5, and TCE = 3). The atrazine data were reported in Kempf and Brusseau (2009) and the TCE data were reported in Schnaar and Brusseau (2014).	35
Figure 2.5. Simulated breakthrough curves for PFOS and TCE transport in the Eustis soil for system conditions representing a factor of 100 increase in residence time compared to the conditions used for the miscible-displacement experiments. See the main text for more information.	38

ABSTRACT

Miscible-displacement experiments were conducted to investigate the transport of two emerging contaminants of interest: graphene nanoparticles and perfluorooctanesulfonic acid (PFOS), a representative per and polyfluoroalkyl substance (PFAS).

The study of graphene transport focuses on the effect of different factors such as surfactant type, soil type, flow rate, pristine/oxidized form on graphene transport. Breakthrough occurred at 1 pore volume, coincident with a nonreactive tracer and consistent with standard colloid transport theory. The effluent concentrations plateaued at levels lower than the input concentration, indicating irreversible attachment to the solid surface. The observed increasing relative concentration plateau indicated the existence of colloid blocking phenomenon. Greater retention was observed for SDBS-dispersed graphene versus Tween 80-graphene, in Vinton soil versus in sand, at a lower flow rate, and for pristine graphene.

Both experiments and mathematical model simulations were used to investigate PFOS transport in two soils and three aquifer sediments. The breakthrough curves exhibited nonideal transport behavior, with asymmetry and extended tailing. The widely used two-domain sorption kinetics model provides good simulations for the experiment with standard input and elution time but cannot fit the long tailing with extended time. A continuous-distribution multi-rate model that has a better resolution for the pore/grain-scale can provide good simulations for the extended elution tailing.

CHAPTER 1. INTRODUCTION

Emerging contaminants, or contaminants of emerging concern, include a wide range of chemicals that have potential risk for human health yet have not been completely regulated due to their newly found existence and toxicity. Graphene (a nanoparticle) and PFOS are two of them which have gained increasing environmental concern in recent years. The present study investigated their transport and retention behavior under saturated conditions.

1.1 Transport of Graphene and Graphene Oxide in Saturated Porous Media

1.1.1 Research Purpose

Graphene is a two-dimensional (2D) material comprising of a monolayer of carbon atoms. Its existence was only theoretical until 2004, when the scientists Geim and Novoselov successfully produced free standing graphene exfoliated from graphite. They were awarded the Nobel Prize in Physics in 2010 for this groundbreaking work. Since then, graphene has obtained more and more research interest. With so many great properties due to its unique 2D structure, most of the current research is focusing on the potential applications of this new material or developing better methods for large scale production of defect-free graphene. Meanwhile, the toxicity of graphene nanoparticles in animal tissues has been demonstrated and the environmental concern of graphene nanoparticles has also been arising. However, the transport and fate of graphene is still unclear and very few miscible displacement studies have been reported. Liu et al. (2015) compared the transport of graphene dispersed by a cationic surfactant, cetyltrimethylammonium bromide (CTAB) and an anionic surfactant, sodium dodecylbenzene sulfonate (SDBS) in saturated

quartz sand. Su et al. (2017) investigated the effects of ionic strength on transport of graphene in saturated quartz sand. These studies proposed some potential mechanisms involved in graphene transport in saturated quartz sand. Comparing more variables under various conditions would be necessary to have a better understanding of graphene transport.

1.1.2 Literature Review

Graphene and Graphene Oxide Nanoparticles

Graphene is a single layer of carbon atoms arranged in a hexagonal lattice due to sp^2 hybridization. It is the building block of other graphitic allotropes. The 2D graphene can be wrapped up into a 0D fullerene, rolled into a carbon nanotube, or stacked into a 3D graphite (Geim and Novoselov, 2007). Graphene has aromaticity, but is different from benzene (Popov et al., 2012).

Graphene is more than 100 times stronger than the strongest steel, yet very light, with a density of 0.77 mg/m^2 , equivalent to 2.3 g/cm^3 , considering the thickness of single-layer graphene is 0.335 nm (Ni et al., 2007). It has a higher electrical conductivity and lower resistance than the ubiquitous copper wire. Its 2D form is almost transparent and transmits 97% of the light.

Graphene oxide (GO) is the oxide of graphene, with oxygen-bearing functional groups on the surface and edge of the nanoparticle. It has been studied for more than a hundred years due to a relatively easy method for production. First developed by Brodie in 1859, and modified by Hummers and Offeman (1958), it is still a popular method to produce GO. The method involves oxidizing graphite with a mixture of potassium chlorate

and a concentrated acid, dispersing the oxidized graphite into water and obtaining the dispersed and exfoliated monolayer GO. This method has also been used for producing graphene, with an additional reduction of the graphene oxide. While the graphene produced with this method still contains some oxygen-bearing functional groups on the edge and some structure defect, it is also named reduced graphene oxide (rGO), to differentiate it from pristine graphene. Lotya et al. (2009) proposed that liquid exfoliation method can be used to produce pristine graphene. They exfoliated graphite powder in aqueous phase into graphene nanoparticles by adding the surfactant SDBS under sonication, followed by centrifugation. Both GO and rGO can disperse into the water by itself. Graphene can only disperse in select organic solvents or in water with the help of surfactants.

Surfactant-dispersed Graphene Suspension

Surfactants are amphiphilic compounds with a hydrophobic tail and hydrophilic head. They can decrease the surface tension of a solution and facilitate dispersal of nanoparticles. Like dissolves like, when added into water, the hydrophobic tail, usually a long hydrocarbon chain, will try to escape from the bulk solution, while the hydrophilic head, with large polarizability, prefers to stay in the solution. Therefore, the surfactant is prone to distribute at the surface of water, head immersed in water and tail sticking outward to the air. As more and more surfactants are added and the surface of water is occupied with surfactants, newly added surfactant has to stay in the bulk solution. Continuing adding surfactants will result in the aggregation of surfactants and the formation of micelles. Figure 3 listed three typical micelle formations: spherical, cylindrical and bilayer, with

hydrophobic tail inward and hydrophilic head outward. The hydrophobic compound would be wrapped inside the micelle in aqueous phase.

Surfactant dispersed graphene has been found to have a wide application. Quinn et al. (2018) proposed the surfactant-dispersed graphene suspension can be used for inducing controllable drug release and ablative therapies for tumor and necrosis due to its biocompatibility, strong absorption in the near-infrared (NIR), and high tolerance for extreme temperature. Surfactant modified graphene can be added into nitrile latex nanocomposite to optimize its characteristics (Raghavendrakumar and Suresh, 2019), Pluronic F108 (a nonionic surfactant) dispersed graphene can efficiently stabilize liquid-air foams for mineral froth flotation and wastewater treatment (Sham and Notley, 2016). Ionic surfactant dispersed graphene can be used to adsorb dye pollutants with counterions from aqueous solutions (Sham and Notley, 2018). Xu et al. (2019) studied the adsorption of hydrogen by SDBS dispersed graphene and proposed a potential method for storing hydrogen energy. Higashi et al. (2016) synthesized a polymerized surfactant to disperse the graphene nanoparticles. These surfactants can be immobilized on the graphene surface through crosslinker, ensuring a stable dispersion. They also proved that the surfactant-dispersed graphene suspension can be used as conductive graphene ink. Hu and Liu (2012) presented enhanced performance of the sensor using graphene modified electrode in the presence of an anionic surfactant, sodium dodecyl sulfate (SDS). Surfactant facilitated graphene suspension can be used to make nanocomposites which obtain larger/reversible lithium storage, higher conductivity, higher specific capacitance, reliable endurance and thus better performance in electronic field (Huang et al., 2013; Hsieh et al., 2015; Liu et al., 2018; Sukumaran et al., 2018; Pakulski et al., 2019). Surfactant facilitated graphene

composite can also be used to degrade cationic-anionic dye pollutants (Nguyen and Oh, 2018).

Surfactant type and their interaction with graphene may have an effect on the characteristic of graphene suspension and their potential application. Lin et al. (2011) studied the interaction between graphene nanoparticles and an anionic surfactant, sodium cholate (SC) and observed the hydrophobic groups of SC are adsorbed onto the surface of graphene and the hydrophilic groups are directed away from graphene into the bulk suspension. The adsorbed hydrophobic parts prefer to arrange themselves side by side. Arunachalam and Vasudevan (2017) probed the interaction between CTAB and graphene nanoparticles and found the hydrophobic chains of CTAB are weakly adsorbed to the surface of graphene while exchanging rapidly with the free surfactant in the bulk suspension. Smaller surfactants such as SDS can be adsorbed onto graphene more than large ones and thus stabilize graphene better (Poorsargol et al., 2019).

The preceding overview illustrates that many graphene applications involve the use of surfactants to facilitate production and use. Hence, it is to be expected that some manufacturing disposed-product waste streams will contain surfactant in conjunction with graphene. It is important therefore to investigate graphene transport in the presence of surfactant.

Colloid Filtration Theory

Colloid filtration theory was initially developed by Yao et al. (1971) used for modelling water and waste water filtration processes, which is analogous to and often used for analyzing attachment of colloidal particles to the surface of porous media (a single

grain, or collector) during colloid transport under saturated, steady-state conditions. Three mechanisms are involved in removal of suspended particles from flowing water, i.e., attachment of suspended particles onto the media surface: sedimentation, interception, and diffusion, based on the size and density of the transported colloidal particles. Single collector efficiency (η) is defined as the probability of a transported particle striking a collector, which is the sum of three components representing the three attachment mechanisms. Each component can be calculated with the analytical results provided by Levich (1962) and Yao et al. (1971). Attachment efficiency coefficient (α) is defined as the probability of an attachment onto a collector caused by the contact between a particle and a collector. α and η are related to the characteristics of a given colloid transport system in an equation:

$$\ln \frac{C}{C_0} = -\frac{3}{2}(1-n)\alpha\eta \frac{L}{d_c}$$

where $\frac{C}{C_0}$ is the recovery of the colloids, n is the porosity of the porous media, L is the length of the packed column, d_c is the mean diameter of the grain size.

According to colloid filtration theory, increasing flow velocity will not influence α (Ryan and Elimelech, 1996). Shen et al. (2010) added a supplement that once flow velocity increases to a critical value, α will decrease with increasing flow velocity. However, the adverse pattern (i.e., increased α with increasing flow velocity) have also been observed for some carbon nanomaterials (Lecoanet and Wiesner, 2004; Zhang et al., 2018).

$\alpha\eta$ is called removal efficiency. It can be used to analyze the retention of nonspherical particles such as bacteria of different species (Bolster et al., 2006) and

graphene oxide nanosheets (Lanphere et al., 2014). Larger values reflect reduced transport in porous media.

1.2 Nonideal Transport and Extended Elution Tailing of PFOS in Soil and Aquifer Sediment

1.2.1 Research Purpose

Per- and polyfluoroalkyl substances (PFASs) have been widely used as fast food packages, non-stick coatings, fire-fighting foams for the past few decades. Nowadays, they have been detected in surface water, sediments, soils, groundwater and wastewater globally due to the excess use and uncontrolled release (Zareitalabad et al., 2013). The hydrocarbon chains of PFAS molecules are highly or fully fluorinated. The strong carbon-fluorine bonds make PFAS nonbiodegradable and persistent in the environment (Key et al., 1997). Recently, the human health concern has also arisen as the toxicity and bioaccumulation of PFAS have been confirmed. PFOS and PFOA (see their molecular formulas in Figure 4) are most widely used and studied PFASs. USEPA (2016) established a lifetime health advisory level (HAL) of 70 ng/L for the combined concentrations of them in drinking water. The U.S. Agency for Toxic Substances and Disease Registry released a report last year suggesting levels should be in the range of ~20 ng/L (ASTDR, 2018). These risk levels are much lower than the maximum contaminant levels established for other common contaminants such as arsenic (10 µg/L) and trichloroethene (5 µg/L).

Understanding the transport and retention behavior would help evaluate the risks of PFAS contamination in groundwater and design effective remediation methods. However, until now, only limited studies on PFOS transport have been reported. McKenzie

et al. (2015) investigated the transport of perfluorooctanoic acid (PFOA), perfluorooctane sulfonic acid (PFOS), and other PFAS in a loamy sand. Brusseau and colleagues (Lyu et al., 2018; Brusseau et al., 2019) investigated the transport of PFOA and PFOS in quartz sands and a soil. Lv et al. (2018) examined the transport of PFOA in quartz sand and in limestone. Aly et al. (2018) conducted column experiments to test the effect of two amendments to enhance sorption of PFOS onto quartz sand. The majority of the prior research has focused on PFAS transport in ideal, geochemically simple porous media. It is anticipated that the magnitude and complexity of PFAS adsorption will be greater for transport in soils and aquifer materials. Investigating transport in more soils and aquifer materials would be helpful to study the more complicated retention mechanisms for PFOS transport in groundwater.

In this study, miscible-displacement experiments with several soils and aquifer materials of different geochemical properties were conducted to investigate the transport and retention of PFOS. Some sets of experiments were treated with extended elution time to investigate the potential extensive elution tailing of breakthrough curves (BTCs) which reflects nonideal sorption/desorption. Two mathematical models incorporating different sorption/desorption kinetics were used to determine which one is the dominant factor.

1.2.2 Literature Review

PFASs

PFASs are a large group of highly fluorinated hydrocarbon compounds. Among them, perfluoroalkyl sulfonates (PFASs) and perfluoroalkyl carboxylates (PFCAs) are

most commonly studied. They are very recalcitrant in the environment and have been detected in air, soils, waters, animals and humans (Jahnke et al., 2007; Giesy and Kannan, 2001; Kannan et al., 2004). Its bioaccumulation has been reported all over the world among a variety of plants and animals (Haukas et al., 2007; Pedersen et al., 2015; Cervený et al., 2018; Karnjanapiboonwong et al., 2018; Ghisi et al., 2019). Some neutral, volatile PFASs such as fluorotelomer alcohols (FTOHs), perfluoroalkyl sulfonamides (FASAs), perfluoroalkyl sulfonamidoethanols (FASEs) and have been found to be able to transform into PFCAs and PFSAAs through (bio)degradation on aerobic conditions (Ellis et al., 2004; Martin et al., 2006; Rhoads et al., 2008; Ahrens, 2011). As fluorine has the smallest size of all the halogen element, it has the strongest electronegativity. And the carbon-fluorine covalent bond is much shorter and stronger than other carbon-halogen bonds. This renders PFASs to be stable and persistent in the environment.

Adsorption of PFAS is influenced by solution chemistry, and the properties of PFAS and the adsorbents (Du et al., 2014). Changing solution chemistry often affects the electrostatic interactions between PFAS and adsorbents. Increasing pH decreases the PFAS adsorption (Yu et al., 2008; Tang et al., 2010; Wang and Shih, 2011). Existence of inorganic divalent cations can increase sorption of anionic PFAS by bridging them with the negatively charged adsorbent surfaces (You et al., 2010; Jeon et al., 2011; Chen et al., 2012) while adding inorganic anions can decrease PFAS sorption through competition for sorption sites (Zhang et al., 2011; Wang et al., 2012). PFAS molecules have different hydrophobicity based on their size and functional groups, which renders them different adsorption capacities when hydrophobic interaction is involved in the sorption process. Perfluoroalkyl sulfonates (PFSAAs) are more hydrophobic than perfluoroalkyl carboxylates

(PFCAs) when containing the same carbon numbers (Higgins and Luthy, 2006; Yu and Hu, 2011; Zhao et al., 2011; Punyapalakul et al., 2013). For PFASs with the same functional group, longer hydrocarbon (C-F) chains relates to higher hydrophobicity and higher adsorption capacity (Zhou et al, 2010; Xiao et al., 2011; Zhang et al., 2013). Smaller PFAS molecules encounter less steric hindrance which is favorable for adsorption (Yu et al., 2009; Deng et al., 2010). Grain/pore size plays an important role in adsorption kinetics of PFAS. Larger specific surface areas relate to greater adsorption capacity (Chen et al., 2011; Deng et al., 2015). Organic matter and metal-oxide constituents on adsorbent surfaces are also favorable for PFAS adsorption (You et al., 2010; Ahrens et al., 2011; Karoyo and Wilson, 2013; Zhou et al., 2013).

In summary, the adsorption of PFAS by soils, sediments, and aquifer materials is more complicated than it is for typical hydrophobic contaminants studied in the past. Thus, it is critical to examine adsorption behavior for a range of porous media properties. Inspection of the literature reveals at least 37 prior studies have been conducted to examine PFAS adsorption by soils, sediments, or aquifer materials. This number does not count the several tens of articles dealing with PFAS adsorption by granular activated carbon, clay minerals, or metal-oxide minerals. For all but five of the 37 studies, the organic carbon contents of the media were larger than 0.1%, with most ranging near or above 1%. It is important to investigate PFAS adsorption for media with lower organic carbon contents, as these are typical for aquifers and deeper vadose zones. For example, only one prior study has been conducted using aquifer material.

Almost all of the adsorption studies mentioned in the preceding paragraph were conducted using batch methods. As discussed in section 1.2.1, only five prior miscible-

displacement (column) studies have been conducted to specifically examine PFAS transport in porous media. All but one of these used simple, geochemically homogeneous media such as quartz sand. In addition, to our knowledge, no one has investigated the extended elution tailing of PFAS specifically. It is important to characterize and quantify this phenomenon, as the HAL for PFAS is so much lower than most other contaminants.

Two-domain Sorption-kinetics (TDSK) Model

The two-domain theory for sorption assumes that sorption reaches equilibrium instantaneously for part of the domain while remains rate-limited for the other domain (Cameron and Klute, 1977). Equations below describes the nonlinear, rate-limited sorption/desorption with Freundlich isotherm for the two-domain model (Hu and Brusseau, 1998):

$$S_1 = FK_f C^N$$

$$S_2 = (1 - F)K_f C^N$$

$$\frac{dS_2}{dt} = k_2[(1 - F)K_f C^N - S_2]$$

C – solute concentration in solution ($M L^{-3}$)

S_1 – solute concentration in sorbed phase in the instantaneous domain ($M M^{-1}$)

S_2 – solute concentration in sorbed phase in the rate-limited domain ($M M^{-1}$)

K_f – Freundlich sorption coefficient ($L^{3N} M^{-N}$)

N – Freundlich exponent

F – fraction of sorbent for instantaneous sorption

k_1, k_2 – first-order adsorption, desorption rate coefficients (T^{-1})

One-dimensional transport under steady state flow using the two-domain assumption (Brusseau, 1995) can be expressed as:

$$(1 - \beta)R \frac{\partial S^*}{\partial T} = \omega(C^{*N} - S^*)$$

$$\frac{\partial C^*}{\partial T} + (\beta R - 1)NC^{*N-1} \frac{\partial C^*}{\partial T} + \omega(C^{*N} - S^*) = \frac{1}{P} \frac{\partial^2 C^*}{\partial X^2} - \frac{\partial C^*}{\partial X}$$

wherein the dimensionless parameters are defined as follows:

$$C^* = \frac{C}{C_0}$$

$$S^* = \frac{S_2}{(1 - F)K_f C_0^N}$$

$$T = \frac{vt}{L}$$

$$X = \frac{x}{L}$$

$$P = \frac{vL}{D}$$

$$\omega = \frac{k_2(1 - \beta)RL}{v}$$

$$R = 1 + \frac{\rho_b}{\theta_w} K_f C_0^{N-1}$$

$$\beta = \frac{1 + \frac{\rho_b}{\theta_w} FK_f C_0^{N-1}}{R}$$

C_0 – solute input concentration ($M L^{-3}$)

v – mean pore-water velocity ($L T^{-1}$)

L – column length (L)

x – distance (L)

P – Peclet number

D – dispersion coefficient

ω – Damkohler number

R – retardation factor

ρ_b – bulk density ($M L^{-3}$)

θ_w – volumetric water content

β – fraction of retardation that is effectively instantaneous

TDSK has been successfully used to simulate a diverse range of organic and inorganic compounds such as trichloroethene (TCE), bisphenol-A (BPA), sulfadiazine (SDZ), arsenate (As, V), cadmium (Cd) for a variety of soils (Tsang et al., 2007; Yolcubal and Akyol, 2008; Wehrhan et al., 2010; Akyol et al., 2011; Zakari et al., 2016).

Continuous-distribution Multi-rate (CDMR) Model

Extensive elution tailing of BTCs caused by nonideal sorption/desorption has been observed for a lot of miscible-displacement studies on hydrophobic organic compounds (HOCs) including TCE, tetrachloroethene (PCE) and atrazine with different soils and sediments with an extended elution time (Johnson et al., 2003; Russo et al., 2010; Brusseau et al., 2012; Schnaar and Brusseau, 2014; Akyol, 2015). In these studies, TDSK model could not obtain good simulations, while the CDMR model has been proved to fit the elution tailings very well. The CDMR model takes into account the pore/grain-scale heterogeneity by employing a continuous distribution for sorption/desorption domains. The first-order rate coefficient for the sorption/desorption kinetics, k_2 , is defined as a random variable with a ln-normal distribution (e.g., Johnson et al., 2003):

$$f(k_2) = \frac{1}{\sqrt{2\pi}k_2\sigma_k} \exp\left(-\frac{[\ln(k_2) - \mu]^2}{2\sigma_k^2}\right)$$

where μ is the mean of $\ln(k_2)$, σ_k is the variance of $\ln(k_2)$. Sorption for the equilibrium and rate-limited domains are described as:

$$\frac{\partial S_{eq}}{\partial t} = FK_f C^N \frac{\partial C}{\partial t}$$

$$\frac{\partial S_i}{\partial t} = k_{2i}[(1 - F)K_f C^N - S_i]$$

Incorporate the sorption terms into the advection-dispersion equation:

$$\frac{\partial C}{\partial t} + \frac{\rho_b}{\theta} \frac{\partial S_{eq}}{\partial t} + \frac{\rho_b}{\theta} \sum_{i=1}^m f_i(k_{2i}) \frac{\partial S_i}{\partial t} = -v \frac{\partial C}{\partial x} + D \frac{\partial^2 C}{\partial x^2}$$

where m is the total number of domains, set depending on the experiment conditions.

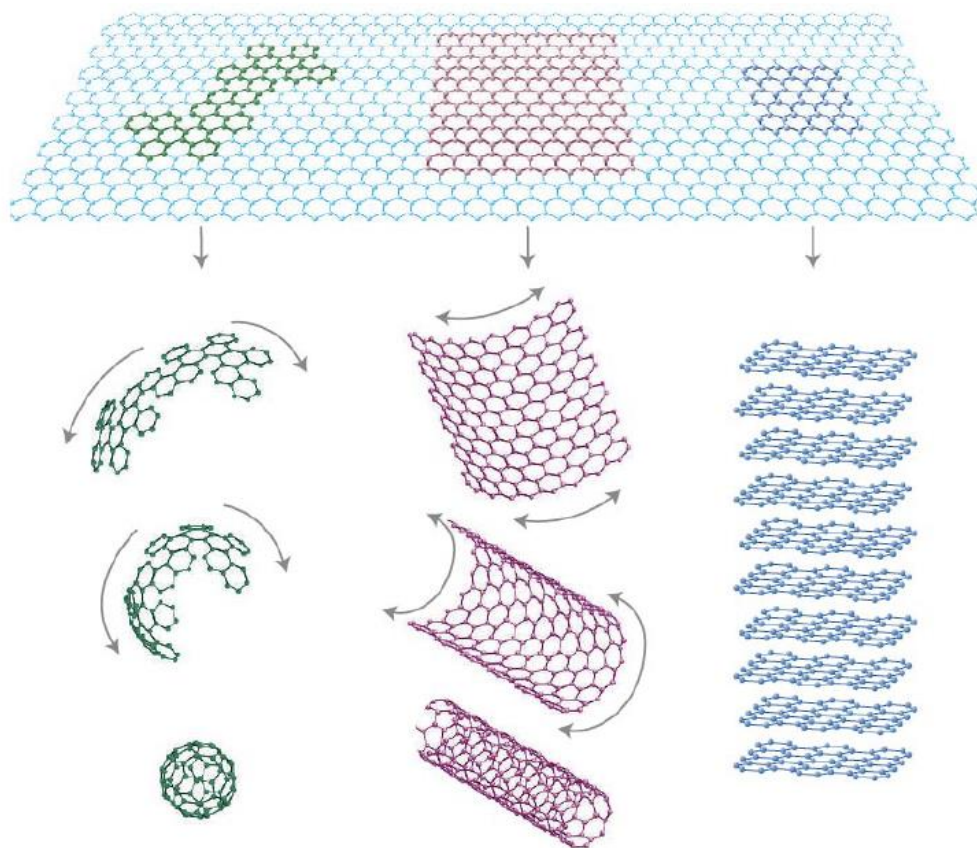
FIGURES

Figure 1.1. Graphene (top) as a building material for other carbon materials such a 0-dimensional fullerene (bottom left), 1-dimensional carbon nanotube (bottom middle), and 3-dimensional graphite (bottom right). (Geim and Novoselov, 2007).

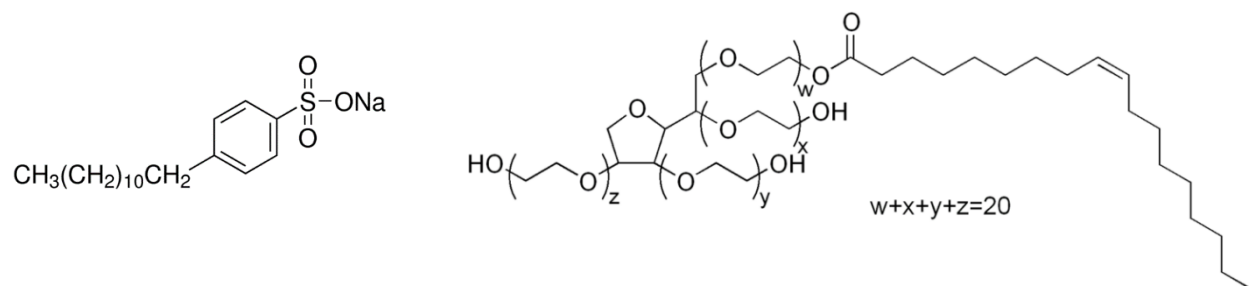


Figure 1.2. Molecular formulas of an anionic surfactant, SDBS (left) and a nonionic surfactant, Tween 80 (right).

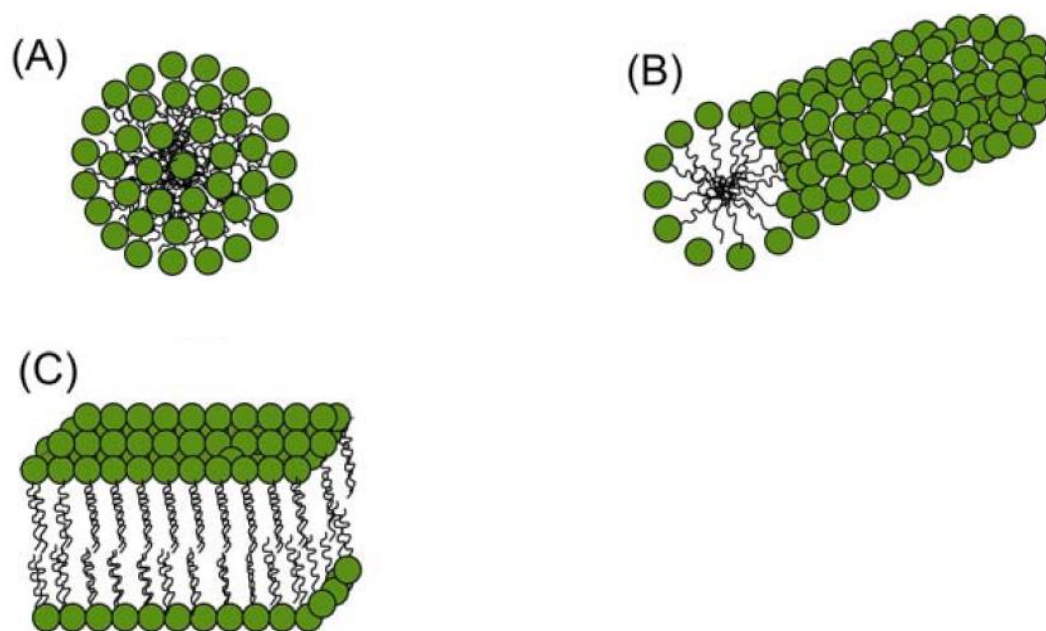


Figure 1.3. Three typical micelle formations: (A) spherical, (B) cylindrical, and (C) bilayer (Lugo, 2010).

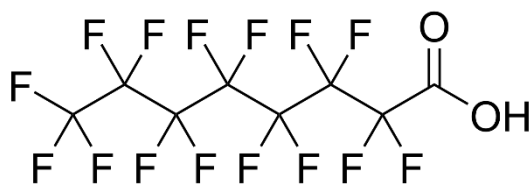
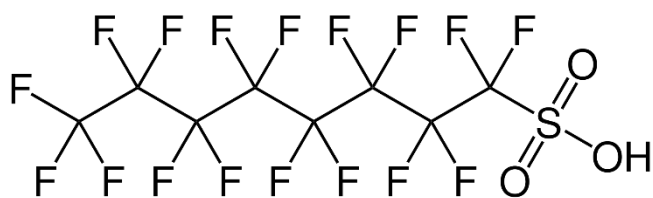


Figure 1.4. Molecular formulas for PFOS (top) and PFOA (bottom).

CHAPTER 2. PRESENT STUDY

2.1 Transport of Graphene and Graphene Oxide in Saturated Porous Media

Note that this component of the study is presented in full in Appendix A.

2.1.1 Materials and Methods

Graphene or graphene oxide nanoparticles were dispersed into the water with or without surfactant (SDBS or Tween 80). Acrylic columns (15 cm long, 2.6 cm in diameter) were packed with 20/30 sand or Vinton soil. A piston pump (Fluid Metering, Inc., US) was used to provide a flow rate of 1 mL/min or 0.17 mL/min (equivalent to a pore-water velocity of ~30 cm/h or 5 cm/h).

At first, water was injected into the column from the bottom at a very slow flow rate until saturation. A nonreactive tracer, PFBA (120 mg/L), was injected into the column for 3-4 pore volumes (PVs), followed by another 3-4 PVs of water. After this, a background solution (surfactant solution) was injected into the column for several PVs. Then graphene suspension was injected into the column for 3-5 PVs, followed by another 3-5 PVs of background solution.

The effluent samples were collected with a fraction collector (RediFrac, Pharmacia LKB, US) and analyzed with UV-vis spectrophotometry at 430 nm (SDBS-graphene), 226 nm (Tween-graphene), 248 nm (SDBS-graphene oxide), 225 nm (graphene oxide). Colloidal particle size and zeta potential at different phases of the experiment were measured by dynamic light scattering and electrophoretic light scattering, with a Zetasizer Nano (Malvern Instruments, UK).

2.1.2 Summary of the Results

The porous media were homogeneously and hydrodynamic conditions were ideal as the BTCs of nonreactive tracer are sharp and symmetrical, with a recovery close to 100%. The transport data for all of the experiments are presented in Appendix A. An illustrative example is presented in Figure 2.1.

All the BTCs for graphene transport has a breakthrough at 1 PV. Recoveries range from 50-86%, indicating irreversible retention. These results are consistent with the standard colloid transport theory. The relative concentration plateau of all the BTCs for graphene has a slowly increasing trend. This may be caused by the so-called colloid blocking phenomenon (i.e., a decreased attachment potential for colloids later coming in due to the occupied deposition site with colloids attached earlier).

Flow rates, surfactant type, soil type all have an effect on transport and retention of surfactant-dispersed graphene. Greater retention was observed at a lower velocity (larger residence time), in Vinton soil which contains more metal (hydr)oxide versus sand, and for SDBS-graphene versus Tween 80-graphene. We attribute the greater retention for more negatively charged SDBS-graphene to an increase of ionic strength caused by excess SDBS molecules.

Graphene oxide is more mobile and has a higher recovery than graphene, consistent with the fact that graphene oxide contains polar oxygen-bearing functional groups. Recovery of SDBS-graphene oxide decreased by 17% compared to that of graphene oxide at the same condition, which also supports the hypothesis that the excess SDBS molecules may influence the ionic strength of the suspension and the retention of the nanoparticles.

The calculated attachment efficiencies increase with an increasing flow velocity, which is contradict with the classical colloid filtration theory, but consistent with some more recently results for carbon nanoparticles such as fullerene and graphene oxide. This phenomenon may relate to their special shapes.

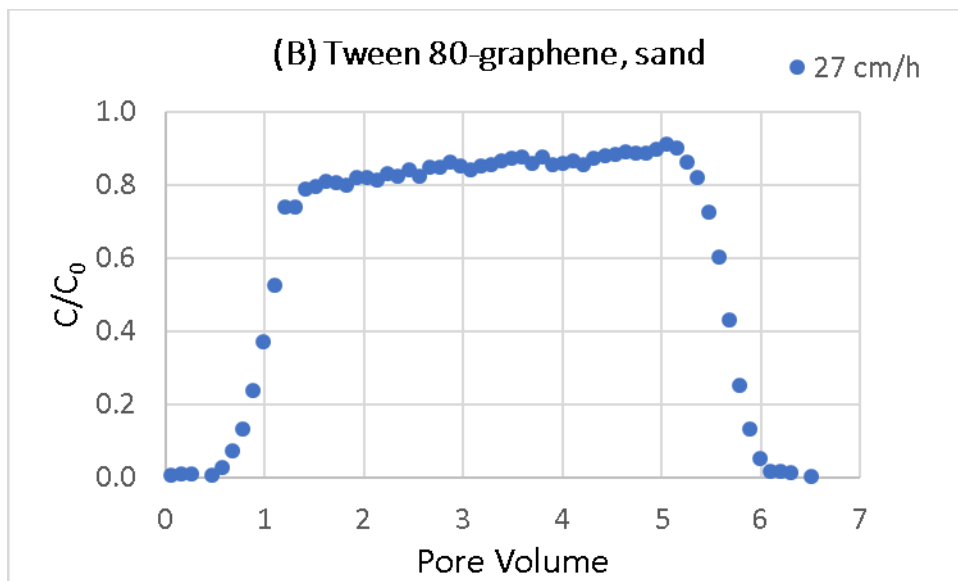


Figure 2.1 Example of graphene transport in a column packed with sand.

2.2 Nonideal Transport and Extended Elution Tailing of PFOS in Soil and Aquifer Sediment

Note that this component of the study is presented in full in Appendix B.

2.2.1 Materials and Methods

Acrylic columns or stainless steel columns (length of 7-20 cm, with an inner diameter of 2-2.5 cm) were packed with five porous media of different geochemical properties--- Vinton soil, Eustis soil, Borden aquifer material, Hanford aquifer material, or AFP 44 aquifer material. Select properties of the media are presented in Table 2.1. The Eustis soil (siliceous, thermic Psammentic Paleudults) is composed primarily of quartz, with small fractions of feldspar (0.5%) and clay minerals (1.7%, essentially all kaolinite). It has a total organic-carbon content of 0.38%, consisting of approximately 37% hard carbon (kerogen and black carbon) and 63% soft carbon (humic/fulvic acids, lipids). It has a relatively low metal-oxide content. The Vinton soil (sandy, mixed, thermic Typic Torrifluent) consists of 54% silica, 36% feldspar, 3% amphibole, and 4.7% clay minerals. The clay minerals consist of similar proportions of kaolinite, vermiculite, and illite, with small fractions of montmorillonite and amorphous silica. It has a lower (0.1%) organic-carbon content and a higher metal-oxide content. The Borden medium was collected from the Canadian AFB Ontario, which is a well-known site for contaminant hydrology field studies. It has low organic carbon and oxide content. The Hanford medium was collected from the Hanford, WA Department of Energy facility. It has a quite high iron oxide content and low organic carbon. The AFP44 medium was collected from the AFP44 site, which is part of the Tucson International Airport Area Superfund site in Tucson, AZ. It has low organic carbon.

Precision HPLC pumps were used to provide a constant flow rate of 1 mL/min (equivalent to a pore-water velocity of 52 cm/h). At first, synthetic groundwater was injected into the column from the bottom at a very slow flow rate until saturation. A nonreactive tracer, PFBA (120 mg/L, dissolved in synthetic groundwater), was injected into the column for 3-4 PVs, followed by another ~10 PVs of synthetic groundwater. After this, 10 mg/L of PFOS solution (dissolved in synthetic groundwater) was injected into the column for ~20 PVs, followed by another ~50 PVs of synthetic groundwater. Experiment sets conducted with such input time and elution time aimed to observe the potential extended elution tailing.

The effluent samples were collected with a fraction collector (RediFrac, Pharmacia LKB). For some experiments, the first ~40 PVs of samples were processed with the methylene blue active substances (MBAS) method (Chitikela et al., 1995) and analyzed with UV-vis spectrophotometry at 650 nm. The remaining samples were analyzed with High Performance Liquid Chromatography tandem mass spectrometry (HPLC-MS).

Two solute transport models incorporating different sorption/desorption kinetics (TDSK and CDMR model) are used to analyze the predominant factor causing the extensive elution tailing.

2.2.2 Summary of the Results

The transport data for all of the experiments are presented in Appendix B. Illustrative examples are provided in Figures 2.2 and 2.3. The ideal breakthrough curves for the nonreactive tracer indicate that the porous media were homogeneous and water flow was uniform.

Prominent arrival-wave and elution-wave tailing were observed for PFOS transport in all media tested, indicating the influence of nonideal sorption/desorption on transport. Extended elution tailing at lower concentrations is in particular observed for PFOS for the two soils (see Figure 2.3 for an illustration). The elution curves for the three aquifer materials exhibit extended tailing as well, but to a lesser extent than for the soils.

The TDSK model can simulate the bulk breakthrough curves, but are not adequate for the extended elution tailing. The CDMR model can fit the long tailing very well. PFOS recoveries are close to 100% for the extended experiment, indicating reversible sorption. The numerical modeling analyses indicated that the impact of nonlinear adsorption was very minor. The results demonstrate that rate-limited adsorption was the primary cause of the observed nonideal transport.

Prior miscible-displacement studies conducted by Brusseau and colleagues examined the transport of several HOCs in the Eustis soil. Representative elution-wave data sets for trichloroethene (TCE) and atrazine are presented in Figure 2.4 along with the PFOS and NRT data. The pore volume (x-axis) is normalized by the respective retardation factors of the compounds to eliminate the effect of differences in the magnitudes of retardation on the extents of tailing. The HOCs have much greater tailing compared to PFOS. It is noteworthy that the retardation factors for TCE and atrazine transport in the Eustis soil are 3 and 3.5, which are slightly smaller than that of PFOS. Hence, for similar magnitudes of sorption and retardation, TCE and atrazine exhibit much greater elution tailing compared to PFOS.

This significant difference in the magnitude of mass-transfer limitations likely reflects differences in the mechanisms mediating sorption/desorption of PFOS versus the

HOCs. Prior research has demonstrated that the sorption/desorption of HOCs in the Eustis soil is controlled by adsorption to and permeation within the soil organic carbon. Conversely, adsorption of PFOS and other PFAS can be influenced significantly by surface interactions with metal oxides and clay minerals as well as interaction with organic carbon.

While the use of organic-carbon normalized adsorption coefficients (K_{oc}) is uncertain for PFAS, they can be calculated to help illuminate potential adsorption mechanisms. Log K_{oc} values are reported in Table 2.1. It is observed that the values are in the range of the mean literature value of 2.8, which is based on adsorption measurements reported for 23 media from seven separate studies. Interestingly, the largest measured log K_{oc} values is for the Hanford medium, which by far has the largest iron oxide content.

Table 2.1. Properties of the Porous Media

Medium	TOC (%)	Fe-oxides (mg/kg)	Mn-oxides (mg/kg)	Total-oxides (mg/kg)	Median Grain Diameter d_{50} (mm)	K_d (cm ³ /g)	Log K_{oc}
Eustis	0.38	310	19	329	0.27	0.76	2.3
Vinton	0.1	1700	130	1830	0.26	0.54	2.7
Borden	0.03	383	70	453	0.21	0.19	2.8
AFP 44	0.06	NA	NA	NA	0.33	0.23	2.6
Hanford	0.06	14620	227	14847	0.25	0.61	3.0
Sand	0.04	14	2.5	16.5	0.35	0.15	2.6

NA = not available

Borden oxide content data from Reinhard et al., 1990.

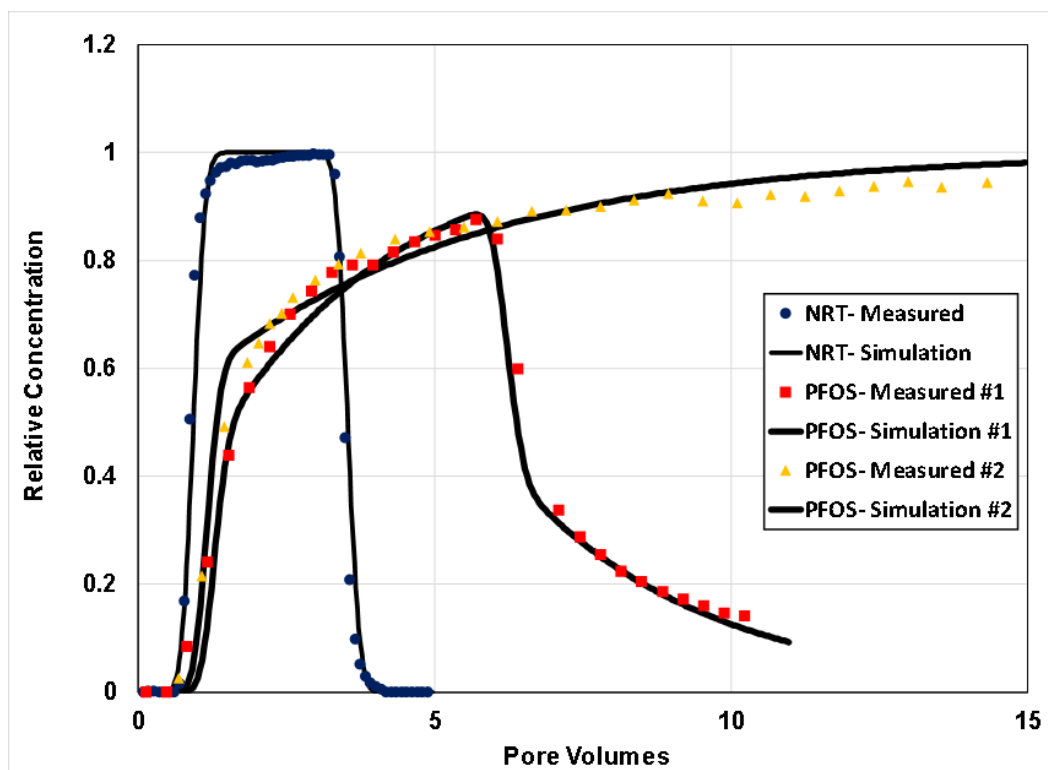


Figure 2.2. Measured and simulated breakthrough curves for transport of the nonreactive tracer (NRT) and PFOS in Vinton soil (Experiments 1a and 1b). The PFOS simulation is produced using a two-domain model that accounts for nonlinear, rate-limited sorption/desorption (expt 1a: $\beta = 0.39$, $\omega = 0.5$; expt 1b: $\beta = 0.46$, $\omega = 0.74$).

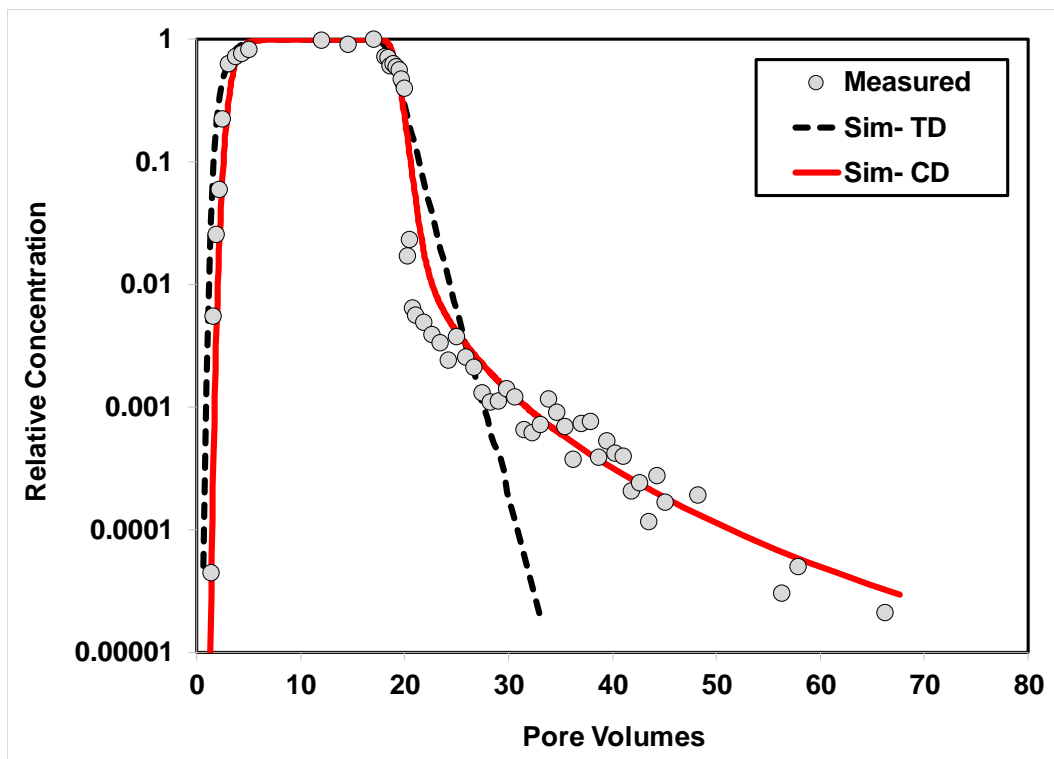


Figure 2.3. Measured and simulated breakthrough curves for transport of PFOS in Vinton soil (Experiment 2). The PFOS simulations are produced using the two-domain sorption-kinetics model (TD) and the continuous-distribution multi-rate model (CD).

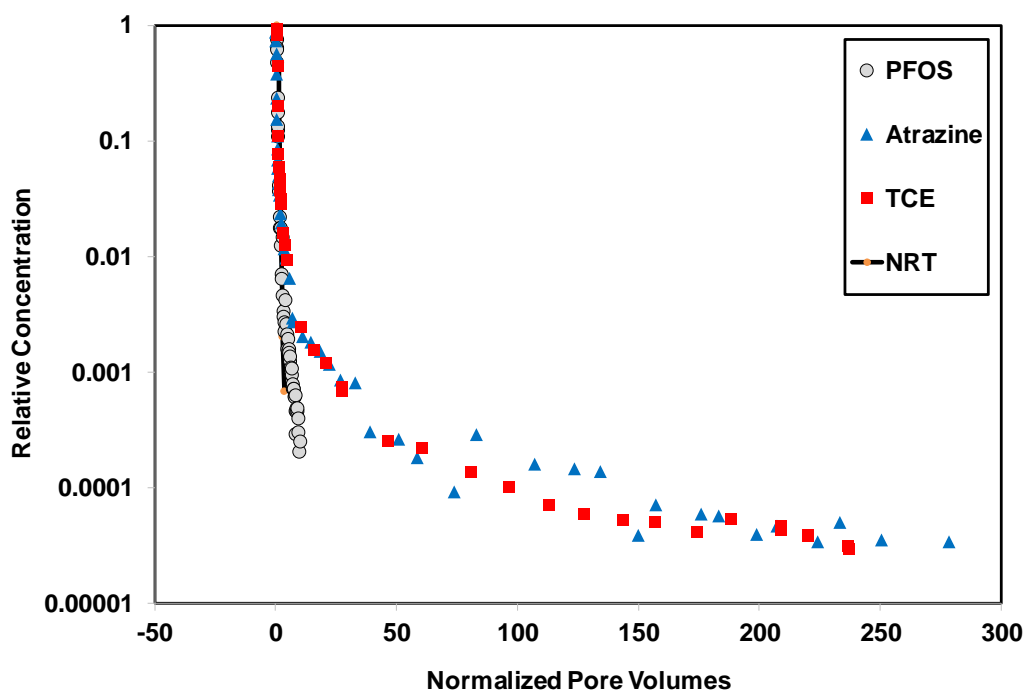


Figure 2.4. Measured elution waves for transport of PFOS, two HOCs, and a non-reactive tracer (NRT) in Eustis soil. The pore volumes are normalized by dividing by the respective retardation factors (NRT = 1, PFOS = 4.2, atrazine = 3.5, and TCE = 3). The atrazine data were reported in Kempf and Brusseau (2009) and the TCE data were reported in Schnaar and Brusseau (2014).

2.3 Conclusions

The miscible-displacement studies for graphene indicate that there is potential for transport in porous media. The transport potential of graphene is greatly influenced by porous-media properties and solution conditions. The presence of surfactants co-disposed with graphene or already present may enhance transport potential.

The study results also have implications for remediation of sites contaminated by graphene wastes. Surfactants play a critical role in graphene transport behavior. Therefore, selecting the appropriate surfactants may be helpful for remediating graphene contamination. In addition, graphene oxides are much more soluble and mobile than graphene. It would be a potential method to remove graphene retained in the soil if graphene can be transferred to its oxide under ambient conditions.

The results reported herein for PFAS transport represent to our knowledge the first examination of the influence of nonideal sorption/desorption processes on PFAS transport in soil with a specific characterization of mass-transfer-limited elution tailing. The breakthrough curves measured for PFOS transport in two soils exhibited extensive elution tailing, indicating that sorption/desorption was significantly nonideal under the extant laboratory conditions. The elution curves for the three aquifer materials exhibited extended tailing, but to a lesser extent than for the soils. Based on the experiments and mathematical modeling, it was determined that the nonideal behavior was caused primarily by rate-limited sorption/desorption.

Standard miscible-displacement studies typically employ pore-water velocities and column lengths that are not representative of field conditions. A question of critical interest is the impact of rate-limited sorption/desorption on PFAS transport at the field scale. This

issue was examined by conducting a set of simulations with the CDMR model wherein the mean pore-water velocity was decreased by a factor of 10 and the system length was increased by a factor of 10, resulting in an overall factor of 100 increase in mean hydraulic residence time. The simulations produced for parameter values representing PFOS and TCE transport in the Eustis soil are presented in Figure 2.5. The extent of elution tailing for PFOS is reduced but not eliminated, whereas TCE elution remains significantly rate limited. These results suggest that rate-limited sorption/desorption for PFOS may be relevant for conditions governed by relatively short residence times, such as for example, in near-well regions of induced-gradient well fields employed for remediation projects.

Concentrations of concern for potential human-health impacts of PFOS and other PFAS are much lower than for other organic contaminants. As noted above, the U.S. EPA recently established a lifetime health advisory level of 70 ng/L for PFOS and PFOA combined for exposure via drinking water. The number of pore volumes required to reach various PFOS concentrations after the start of flushing with PFOS-free solution (i.e., elution pore volumes) can be determined from the PFOS-transport simulation presented in Figure 2.5. PFOS concentrations of 400, 70, 10, and 1 ng/L are attained after approximately 10, 13, 17, and 22 elution pore volumes, respectively. These are substantially larger than the approximately 5 elution pore volumes that would be required if sorption/desorption was instantaneous. It is important to keep in mind that the conditions for the simulations presented in Figure 2.5 represent a factor of 100 increase in hydraulic residence time, including a travel distance of 2 meters. Travel distances and associated residence times are substantially greater for many field sites, and the impact of rate-limited sorption/desorption is likely to become increasingly less significant for these greater residence times as the

difference between the characteristic times of sorption/desorption and field-scale hydraulic-residence times increases. However, the results suggest that rate-limited sorption/desorption could under certain conditions increase the amount of flushing and the associated time required to reduce PFOS concentrations to levels below those associated with human-health concerns.

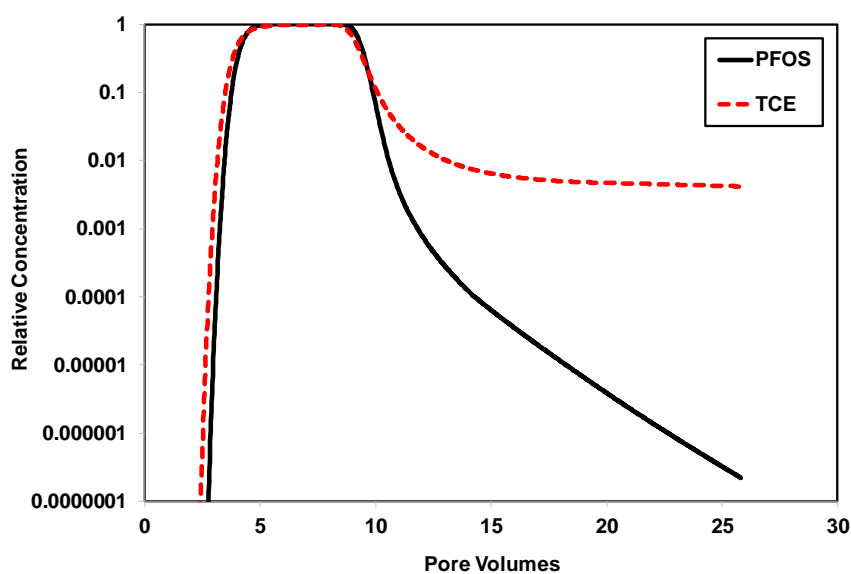


Figure 2.5. Simulated breakthrough curves for PFOS and TCE transport in the Eustis soil for system conditions representing a factor of 100 increase in residence time compared to the conditions used for the miscible-displacement experiments. See the main text for more information.

REFERENCES

- AHRENS, L. 2011. Polyfluoroalkyl compounds in the aquatic environment: a review of their occurrence and fate. *Journal of Environmental Monitoring*, 13, 20-31.
- AHRENS, L., YEUNG, L. W. Y., TANIYASU, S., LAM, P. K. S. & YAMASHITA, N. 2011. Partitioning of perfluorooctanoate (PFOA), perfluorooctane sulfonate (PFOS) and perfluorooctane sulfonamide (PFOSA) between water and sediment. *Chemosphere*, 85, 731-737.
- AKYOL, N. H., YOLCUBAL, I. & YUKSEL, D. I. 2011. Sorption and transport of trichloroethylene in caliche soil. *Chemosphere*, 82, 809-816.
- AKYOL, N. H. 2015. Characterizing and modeling of extensive atrazine elution tailing for stable manure-amended agricultural soil. *Chemosphere*, 119, 1027-1032.
- ALY, Y. H., LIU, C., MCINNIS, D. P., LYON, B. A., HATTON, J., MCCARTY, M., ARNOLD, W. A., PENNELL, K. D. & SIMCIK, M. F. 2018. In Situ Remediation Method for Enhanced Sorption of Perfluoro-Alkyl Substances onto Ottawa Sand. *Journal of Environmental Engineering*, 144, 9.
- ARUNACHALAM, V. & VASUDEVAN, S. 2017. Probing Graphene-Surfactant Interactions in Aqueous Dispersions with Nuclear Overhauser Effect NMR Spectroscopy and Molecular Dynamics Simulations. *Journal of Physical Chemistry C*, 121, 16637-16643.
- ASTDR (AGENCY FOR TOXIC SUBSTANCES AND DISEASE REGISTRY) 2018. Toxicological Profile for Perfluoroalkyls.
- BOLSTER, C. H., WALKER, S. L. & COOK, K. L. 2006. Comparison of *Escherichia coli* and *Campylobacter jejuni* transport in saturated porous media. *Journal of Environmental Quality*, 35, 1018-1025.
- BRUSSEAU, M. L. 1995. THE EFFECT OF NONLINEAR SORPTION ON TRANSFORMATION OF CONTAMINANTS DURING TRANSPORT IN POROUS-MEDIA. *Journal of Contaminant Hydrology*, 17, 277-291.
- BRUSSEAU, M. L., RUSSO, A. E. & SCHNAAR, G. 2012. Nonideal transport of contaminants in heterogeneous porous media: 9 - Impact of contact time on desorption and elution tailing. *Chemosphere*, 89, 287-292.

- BRUSSEAU, M. L., YAN, N., VAN GLUBT, S., WANG, Y. K., CHEN, W., LYU, Y., DUNGAN, B., CARROLL, K. C. & HOLGUIN, F. O. 2019. Comprehensive retention model for PFAS transport in subsurface systems. *Water Research*, 148, 41-50.
- CAMERON, D. R. & KLUTE, A. 1977. CONVECTIVE-DISPERSIVE SOLUTE TRANSPORT WITH A COMBINED EQUILIBRIUM AND KINETIC ADSORPTION MODEL. *Water Resources Research*, 13, 183-188.
- CERVENY, D., GRABIC, R., FEDOROVA, G., GRABICOVA, K., TUREK, J., ZLABEK, V. & RANDAK, T. 2018. Fate of perfluoroalkyl substances within a small stream food web affected by sewage effluent. *Water Research*, 134, 226-233.
- CHEN, H., ZHANG, C., YU, Y. X. & HAN, J. B. 2012. Sorption of perfluorooctane sulfonate (PFOS) on marine sediments. *Marine Pollution Bulletin*, 64, 902-906.
- CHEN, X., XIA, X. H., WANG, X. L., QIAO, J. P. & CHEN, H. T. 2011. A comparative study on sorption of perfluorooctane sulfonate (PFOS) by chars, ash and carbon nanotubes. *Chemosphere*, 83, 1313-1319.
- CHITIKELA, S., DENTEL, S. K. & ALLEN, H. E. 1995. MODIFIED METHOD FOR THE ANALYSIS OF ANIONIC SURFACTANTS AS METHYLENE-BLUE ACTIVE SUBSTANCES. *Analyst*, 120, 2001-2004.
- DENG, S. B., NIE, Y., DU, Z. W., HUANG, Q., MENG, P. P., WANG, B., HUANG, J. & YU, G. 2015. Enhanced adsorption of perfluorooctane sulfonate and perfluorooctanoate by bamboo-derived granular activated carbon. *Journal of Hazardous Materials*, 282, 150-157.
- DENG, S. B., YU, Q. A., HUANG, J. & YU, G. 2010. Removal of perfluorooctane sulfonate from wastewater by anion exchange resins: Effects of resin properties and solution chemistry. *Water Research*, 44, 5188-5195.
- DU, Z. W., DENG, S. B., BEI, Y., HUANG, Q., WANG, B., HUANG, J. & YU, G. 2014. Adsorption behavior and mechanism of perfluorinated compounds on various adsorbents-A review. *Journal of Hazardous Materials*, 274, 443-454.
- ELLIS, D. A., MARTIN, J. W., DE SILVA, A. O., MABURY, S. A., HURLEY, M. D., ANDERSEN, M. P. S. & WALLINGTON, T. J. 2004. Degradation of

- fluorotelomer alcohols: A likely atmospheric source of perfluorinated carboxylic acids. *Environmental Science & Technology*, 38, 3316-3321.
- ENVIRONMENTAL PROTECTION AGENCY. 2016. Fact sheet-PFOS & PFOA. November 2017. EPA 505-F-17-001.
- GEIM, A. K. & NOVOSELOV, K. S. 2007. The rise of graphene. *Nature Materials*, 6, 183-191.
- GHISI, R., VAMERALI, T. & MANZETTI, S. 2019. Accumulation of perfluorinated alkyl substances (PFAS) in agricultural plants: A review. *Environmental Research*, 169, 326-341.
- GIESY, J. P. & KANNAN, K. 2001. Global distribution of perfluorooctane sulfonate in wildlife. *Environmental Science & Technology*, 35, 1339-1342.
- HAUKAS, M., BERGER, U., HOP, H., GULLIKSEN, B. & GABRIELSEN, G. W. 2007. Bioaccumulation of per- and polyfluorinated alkyl substances (PFAS) in selected species from the Barents Sea food web. *Environmental Pollution*, 148, 360-371.
- HIGASHI, C., FUNASAKI, Y., IGUCHI, H. & MARUYAMA, T. 2016. In situ polymerization of a novel surfactant on a graphene surface for the stable dispersion of graphene in water. *Rsc Advances*, 6, 88244-88247.
- HIGGINS, C. P. & LUTHY, R. G. 2006. Sorption of perfluorinated surfactants on sediments. *Environmental Science & Technology*, 40, 7251-7256.
- HSIEH, A. G., PUNCKT, C. & AKSAY, I. A. 2015. High-Rate Li⁺ Storage Capacity of Surfactant-Templated Graphene-TiO₂ Nanocomposites. *Journal of the Electrochemical Society*, 162, A1566-A1573.
- HU, F. T. & LIU, S. Q. 2012. Enhanced Effects of Surfactant on Sensing of Phenol on a Graphene Nano-sheet Paste Electrode. *International Journal of Electrochemical Science*, 7, 11338-11350.
- HU, M. Q. & BRUSSEAU, M. L. 1998. Coupled effects of nonlinear, rate-limited sorption and biodegradation on transport of 2,4-dichlorophenoxyacetic acid in soil. *Environmental Toxicology and Chemistry*, 17, 1673-1680.
- HUANG, G. C., CHEN, T., CHEN, W. X., WANG, Z., CHANG, K., MA, L., HUANG, F. H., CHEN, D. Y. & LEE, J. Y. 2013. Graphene-Like MoS₂/Graphene Composites:

- Cationic Surfactant-Assisted Hydrothermal Synthesis and Electrochemical Reversible Storage of Lithium. *Small*, 9, 3693-3703.
- HUMMERS, W. S. & OFFEMAN, R. E. 1958. PREPARATION OF GRAPHITIC OXIDE. *Journal of the American Chemical Society*, 80, 1339-1339.
- JAHNKE, A., BERGER, U., EBINGHAUS, R. & TEMME, C. 2007. Latitudinal gradient of airborne polyfluorinated alkyl substances in the marine atmosphere between Germany and South Africa (53 degrees N-33 degrees S). *Environmental Science & Technology*, 41, 3055-3061.
- JEON, J., KANNAN, K., LIM, B. J., AN, K. G. & KIM, S. D. 2011. Effects of salinity and organic matter on the partitioning of perfluoroalkyl acid (PFAs) to clay particles. *Journal of Environmental Monitoring*, 13, 1803-1810.
- JOHNSON, G. R., ZHANG, Z. & BRUSSEAU, M. L. 2003. Characterizing and quantifying the impact of immiscible-liquid dissolution and nonlinear, rate-limited sorption/desorption on low-concentration elution tailing. *Water Resources Research*, 39, 8.
- KANNAN, K., CORSOLINI, S., FALANDYSZ, J., FILLMANN, G., KUMAR, K. S., LOGANATHAN, B. G., MOHD, M. A., OLIVERO, J., VAN WOUWE, N., YANG, J. H. & ALDOUS, K. M. 2004. Perfluorooctanesulfonate and related fluorochemicals in human blood from several countries. *Environmental Science & Technology*, 38, 4489-4495.
- KARNJANAPIBOONWONG, A., DEB, S. K., SUBBIAH, S., WANG, D. G. & ANDERSON, T. A. 2018. Perfluoroalkylsulfonic and carboxylic acids in earthworms (*Eisenia fetida*): Accumulation and effects results from spiked soils at PFAS concentrations bracketing environmental relevance. *Chemosphere*, 199, 168-173.
- KAROYO, A. H. & WILSON, L. D. 2013. Tunable macromolecular-based materials for the adsorption of perfluorooctanoic and octanoic acid anions. *Journal of Colloid and Interface Science*, 402, 196-203.
- KEY, B. D., HOWELL, R. D. & CRIDDLE, C. S. 1997. Fluorinated organics in the biosphere. *Environmental Science & Technology*, 31, 2445-2454.

- KEMPF, A. & BRUSSEAU, M. L. 2009. Impact of non-ideal sorption on low-concentration tailing behavior for atrazine transport in two natural porous media. *Chemosphere*, 77, 877-882.
- KEY, B. D., HOWELL, R. D. & CRIDDLE, C. S. 1997. Fluorinated organics in the biosphere. *Environmental Science & Technology*, 31, 2445-2454.
- LANPHERE, J. D., ROGERS, B., LUTH, C., BOLSTER, C. H. & WALKER, S. L. 2014. Stability and Transport of Graphene Oxide Nanoparticles in Groundwater and Surface Water. *Environmental Engineering Science*, 31, 350-359.
- LECOANET, H. F. & WIESNER, M. R. 2004. Velocity effects on fullerene and oxide nanoparticle deposition in porous media. *Environmental Science & Technology*, 38, 4377-4382.
- LIN, S. C., SHIH, C. J., STRANO, M. S. & BLANKSCHTEIN, D. 2011. Molecular Insights into the Surface Morphology, Layering Structure, and Aggregation Kinetics of Surfactant-Stabilized Graphene Dispersions. *Journal of the American Chemical Society*, 133, 12810-12823.
- LIU, L., GAO, B., WU, L., SUN, Y. Y. & ZHOU, Z. H. 2015. Effects of surfactant type and concentration on graphene retention and transport in saturated porous media. *Chemical Engineering Journal*, 262, 1187-1191.
- LIU, L., LI, Y., E, T., JIANG, Z. G., YANG, S. Y., XU, J. S. & QIAN, J. H. 2018. Surfactant-assisted titanium dioxide/graphene composite for enhanced conductivity. *Materials Chemistry and Physics*, 217, 365-370.
- LOTYA, M., HERNANDEZ, Y., KING, P. J., SMITH, R. J., NICOLSI, V., KARLSSON, L. S., BLIGHE, F. M., DE, S., WANG, Z. M., MCGOVERN, I. T., DUESBERG, G. S. & COLEMAN, J. N. 2009. Liquid Phase Production of Graphene by Exfoliation of Graphite in Surfactant/Water Solutions. *Journal of the American Chemical Society*, 131, 3611-3620.
- LV, X. Y., SUN, Y. Y., JI, R., GAO, B., WU, J. C., LU, Q. S. & JIANG, H. 2018. Physicochemical factors controlling the retention and transport of perfluorooctanoic acid (PFOA) in saturated sand and limestone porous media. *Water Research*, 141, 251-258.

- LYU, Y., BRUSSEAU, M. L., CHEN, W., YAN, N., FU, X. R. & LIN, X. Y. 2018. Adsorption of PFOA at the Air-Water Interface during Transport in Unsaturated Porous Media. *Environmental Science & Technology*, 52, 7745-7753.
- MARTIN, J. W., ELLIS, D. A., MABURY, S. A., HURLEY, M. D. & WALLINGTON, T. J. 2006. Atmospheric chemistry of perfluoroalkanesulfonamides: Kinetic and product studies of the OH radical and Cl atom initiated oxidation of N-ethyl perfluorobutanesulfonamide. *Environmental Science & Technology*, 40, 864-872.
- MCKENZIE, E. R., SIEGRIST, R. L., MCCRAY, J. E. & HIGGINS, C. P. 2015. Effects of Chemical Oxidants on Perfluoroalkyl Acid Transport in One-Dimensional Porous Media Columns. *Environmental Science & Technology*, 49, 1681-1689.
- NGUYEN, D. C. T. & OH, W. C. 2018. Ternary self-assembly method of mesoporous silica and Cu₂O combined graphene composite by nonionic surfactant and photocatalytic degradation of cationic-anionic dye pollutants. *Separation and Purification Technology*, 190, 77-89.
- PAKULSKI, D., GORCZYNSKI, A., CZEPA, W., LIU, Z. Y., ORTOLANI, L., MORANDI, V., PATRONIAK, V., CIESIELSKI, A. & SAMORI, P. 2019. Novel Keplerate type polyoxometalate-surfactant-graphene hybrids as advanced electrode materials for supercapacitors. *Energy Storage Materials*, 17, 186-193.
- PEDERSEN, K. E., BASU, N., LETCHER, R., GREAVES, A. K., SONNE, C., DIETZ, R. & STYRISHAVE, B. 2015. Brain region-specific perfluoroalkylated sulfonate (PFSA) and carboxylic acid (PFCA) accumulation and neurochemical biomarker Responses in east Greenland polar Bears (*Ursus maritimus*). *Environmental Research*, 138, 22-31.
- POORSARGOL, M., ALIMOHAMMADIAN, M., SOHRABI, B. & DEHESTANI, M. 2019. Dispersion of graphene using surfactant mixtures: Experimental and molecular dynamics simulation studies. *Applied Surface Science*, 464, 440-450.
- POPOV, I. A., BOZHENKO, K. V. & BOLDYREV, A. I. 2012. Is graphene aromatic? *Nano Research*, 5, 117-123.
- PUNYAPALAKUL, P., SUKSOMBOON, K., PRARAT, P. & KHAODHIAR, S. 2013. Effects of Surface Functional Groups and Porous Structures on Adsorption and

- Recovery of Perfluorinated Compounds by Inorganic Porous Silicas. *Separation Science and Technology*, 48, 775-788.
- QUINN, M. D. J., WANG, T. & NOTLEY, S. M. 2018. Surfactant-exfoliated graphene as a near-infrared photothermal ablation agent. *Biomedical Physics & Engineering Express*, 4, 14.
- RAGHAVENDRAKUMAR, R. & SURESH, K. I. 2019. Effect of Amphiphilic Polymer Modified Graphene Surfactant on the Thermal, Viscoelastic and Tensile Properties of Nitrile Latex Nanocomposites. *Journal of Macromolecular Science Part B-Physics*, 58, 489-504.
- RHOADS, K. R., JANSSEN, E. M. L., LUTHY, R. G. & CRIDDLE, C. S. 2008. Aerobic biotransformation and fate of N-ethyl perfluorooctane sulfonamidoethanol (N-EtFOSE) in activated sludge. *Environmental Science & Technology*, 42, 2873-2878.
- RUSSO, A., JOHNSON, G. R., SCHNAAR, G. & BRUSSEAU, M. L. 2010. Nonideal transport of contaminants in heterogeneous porous media: 8. Characterizing and modeling asymptotic contaminant-elution tailing for several soils and aquifer sediments. *Chemosphere*, 81, 366-371.
- SCHNAAR, G. & BRUSSEAU, M. L. 2014. Nonideal Transport of Contaminants in Heterogeneous Porous Media: 11. Testing the Experiment Condition Dependency of the Continuous Distribution Rate Model for Sorption-Desorption. *Water Air and Soil Pollution*, 225, 9.
- SHAM, A. Y. W. & NOTLEY, S. M. 2016. Foam stabilisation using surfactant exfoliated graphene. *Journal of Colloid and Interface Science*, 469, 196-204.
- SHAM, A. Y. W. & NOTLEY, S. M. 2018. Adsorption of organic dyes from aqueous solutions using surfactant exfoliated graphene. *Journal of Environmental Chemical Engineering*, 6, 495-504.
- SU, Y., GAO, B. & MAO, L. 2017. Concurrent agglomeration and straining govern the transport of C-14-labeled few-layer graphene in saturated porous media. *Water Research*, 115, 84-93.
- SUKUMARAN, S. S., JINESH, K. B. & GOPCHANDRAN, K. G. 2018. Surfactant molecules make liquid phase exfoliated graphene a switching element for resistive

- random access memory applications. *Journal of Materials Science-Materials in Electronics*, 29, 9700-9708.
- TANG, C. Y., FU, Q. S., GAO, D. W., CRIDDLE, C. S. & LECKIE, J. O. 2010. Effect of solution chemistry on the adsorption of perfluorooctane sulfonate onto mineral surfaces. *Water Research*, 44, 2654-2662.
- TSANG, D. C. W., ZHANG, W. & LO, I. M. C. 2007. Modeling cadmium transport in soils using sequential extraction, batch, and miscible displacement experiments. *Soil Science Society of America Journal*, 71, 674-681.
- WANG, F., LIU, C. S. & SHIH, K. M. 2012. Adsorption behavior of perfluorooctanesulfonate (PFOS) and perfluorooctanoate (PFOA) on boehmite. *Chemosphere*, 89, 1009-1014.
- WANG, F. & SHIH, K. M. 2011. Adsorption of perfluorooctanesulfonate (PFOS) and perfluorooctanoate (PFOA) on alumina: Influence of solution pH and cations. *Water Research*, 45, 2925-2930.
- WEHRHAN, A., STRECK, T., GROENEWEG, J., VERECKEN, H. & KASTEEL, R. 2010. Long-Term Sorption and Desorption of Sulfadiazine in Soil: Experiments and Modeling. *Journal of Environmental Quality*, 39, 654-666.
- XIAO, F., ZHANG, X. R., PENN, L., GULLIVER, J. S. & SIMCIK, M. F. 2011. Effects of Monovalent Cations on the Competitive Adsorption of Perfluoroalkyl Acids by Kaolinite: Experimental Studies and Modeling. *Environmental Science & Technology*, 45, 10028-10035.
- XU, T., CHEN, J. Y., YUAN, W. H., LI, L., SUN, Y. J., WU, H. J. & YANG, L. X. 2019. Investigating the hydrogen storage capacity of surfactant modified graphene. *Innovative Solutions for Energy Transitions*, 158, 2112-2117.
- YOLCUBAL, I. & AKYOL, N. H. 2008. Adsorption and transport of arsenate in carbonate-rich soils: Coupled effects of nonlinear and rate-limited sorption. *Chemosphere*, 73, 1300-1307.
- YOU, C., JIA, C. X. & PAN, G. 2010. Effect of salinity and sediment characteristics on the sorption and desorption of perfluorooctane sulfonate at sediment-water interface. *Environmental Pollution*, 158, 1343-1347.

- YU, J. & HU, J. Y. 2011. Adsorption of Perfluorinated Compounds onto Activated Carbon and Activated Sludge. *Journal of Environmental Engineering-Asce*, 137, 945-951.
- YU, Q., DENG, S. B. & YU, G. 2008. Selective removal of perfluorooctane sulfonate from aqueous solution using chitosan-based molecularly imprinted polymer adsorbents. *Water Research*, 42, 3089-3097.
- YU, Q., ZHANG, R. Q., DENG, S. B., HUANG, J. & YU, G. 2009. Sorption of perfluorooctane sulfonate and perfluorooctanoate on activated carbons and resin: Kinetic and isotherm study. *Water Research*, 43, 1150-1158.
- ZAKARI, S., LIU, H., TONG, L., WANG, Y. & LIU, J. F. 2016. Transport of bisphenol-A in sandy aquifer sediment: Column experiment. *Chemosphere*, 144, 1807-1814.
- ZAREITALABAD, P., SIEMENS, J., HAMER, M. & AMELUNG, W. 2013. Perfluorooctanoic acid (PFOA) and perfluorooctanesulfonic acid (PFOS) in surface waters, sediments, soils and wastewater - A review on concentrations and distribution coefficients. *Chemosphere*, 91, 725-732.
- ZHANG, C. J., YAN, H., LI, F., HU, X. & ZHOU, Q. 2013. Sorption of short- and long-chain perfluoroalkyl surfactants on sewage sludges. *Journal of Hazardous Materials*, 260, 689-699.
- ZHANG, C. L., YAN, A., WANG, G., JIN, C., CHEN, Y. H. & SHEN, C. Y. 2018. Impact of Flow Velocity on Transport of Graphene Oxide Nanoparticles in Saturated Porous Media. *Vadose Zone Journal*, 17, 10.
- ZHANG, Q. Y., DENG, S. B., YU, G. & HUANG, J. 2011. Removal of perfluorooctane sulfonate from aqueous solution by crosslinked chitosan beads: Sorption kinetics and uptake mechanism. *Bioresource Technology*, 102, 2265-2271.
- ZHAO, D. M., CHENG, J., VECITIS, C. D. & HOFFMANN, M. R. 2011. Sorption of Perfluorochemicals to Granular Activated Carbon in the Presence of Ultrasound. *Journal of Physical Chemistry A*, 115, 2250-2257.
- ZHOU, Q., DENG, S. B., YU, Q., ZHANG, Q. Y., YU, G., HUANG, J. & HE, H. P. 2010. Sorption of perfluorooctane sulfonate on organo-montmorillonites. *Chemosphere*, 78, 688-694.
- ZHOU, Q., PAN, G. & SHEN, W. 2013. Enhanced sorption of perfluorooctane sulfonate and Cr(VI) on organo montmorillonite: influence of solution pH and uptake

mechanism. Adsorption-Journal of the International Adsorption Society, 19, 709-715.

**APPENDIX A – TRANSPORT OF GRAPHENE AND GRAPHENE OXIDE IN
SATURATED POROUS MEDIA**

Yake Wang

Coauthor: Mark Brusseau*

*Corresponding author: Brusseau@email.arizona.edu

Abstract

Graphene is a single-layer carbon nanomaterial that has drawn significant attention for a variety of applications. The industrial production of graphene is projected to increase greatly in the coming years. However, little is known about its transport and fate in the environment. In this study, Miscible-displacement experiments were conducted to investigate the transport and retention of graphene and graphene oxide in sand and/or Vinton soil. Graphene was dispersed into water with a surfactant solution at a concentration of 2 mg/L. The breakthrough curves for surfactant-dispersed graphene and graphene oxide transport exhibited typical colloid transport behavior, with breakthrough at 1 pore volume (PV) and steady-state plateaus at relative concentrations less than 1. The relative effluent concentration plateau increased slowly towards 1, indicating the existence of a colloid blocking phenomenon. Greater retention was observed in Vinton soil compared to the sand. In addition, retention was greater at lower pore-water velocity and in the presence of SDDBS versus Tween. Graphene oxide displayed a higher mobility compared to graphene.

1. Introduction

Graphene is a relatively new carbon nanomaterial. Since its first isolation from graphite by Geim and Novoselov in 2004, it has received a lot of attention due to its great potential for various applications in material science, electronics, medicine, and others (Novoselov et al., 2012; Li et al., 2017; Geetha Bai et al., 2018). It has many remarkable properties, such as optical transparency, a breaking strength more than 100 times higher than the strongest steel, and a much higher electrical and thermal conductivity than copper (RSAS, 2010).

Various methods for producing defect-free, few-layer, pristine graphene have been developed to meet different markets of graphene application. These methods can be categorized into two main types. One is growth of graphene on some substrate to produce large-area graphene films (Novoselov et al., 2012; Li et al., 2009; Bae et al., 2010). The other is exfoliation of graphite pellets in aqueous phase with the help of surfactants, to obtain small graphene platelets (Blake et al., 2008; Hernandez et al., 2008; Novoselov et al., 2012). The large graphene films, with lateral size to dozens of centimeters, can be used in flexible displays. Small graphene platelets, with a lateral size of several micrometers, dispersed in liquid phase, are versatile and have more practical applications in nanocomposites, conductive inks, batteries, and sensors. (Cheng et al., 2010; Zhu et al., 2010; Novoselov et al., 2012; Ren et al., 2014). As of 2014, the annual production of graphene has reached hundreds of tons, and is still increasing rapidly (Ren et al., 2014).

Studies have reported toxicity of graphene to animal tissues (Sasidharan et al., 2011; Chwalibog et al., 2014). Due to projected production rates, potential for ubiquitous application, and possible toxicity concerns, it is prudent to examine the transport and fate

properties of graphene in environmental media. The transport of graphene oxide in porous media has been examined in several studies (Lanphere et al., 2013; Liu et al., 2013; Qi et al., 2014; Sun et al., 2015; Fan et al., 2015; Zhang et al., 2018; Yin et al., 2019). Conversely, very few investigations of graphene transport are available (Liu et al., 2015; Su et al., 2017). In this work, a series of miscible-displacement experiments was conducted to examine the transport and retention of surfactant-dispersed graphene and graphene oxide nanoparticles in two porous media with similar grain size but different geochemical properties under water-saturated conditions.

2. Materials and Methods

2.1 Materials

Graphene nanoparticles were purchased from Graphene Supermarket (NY, US), with an average lateral size of 4.5 μm (i.e., length and width \sim 4.5 μm), thickness of 12 nm, and purity of 99.2%. Graphene oxide was purchased from ACS Material. It has a diameter of 1-5 μm , a thickness of 0.8-1.2 nm, and purity of 99%. The focus of this work is on systems produced with the second primary method of graphene manufacturing---exfoliation and suspension in surfactant solutions. Two surfactants, sodium 4-dodecylbenzenesulfonate (SDBS) and polyoxyethylene sorbitan monooleate, or polysorbate 80 (Tween 80) were used to disperse graphene nanoparticles. SDBS ($\text{C}_{18}\text{H}_{29}\text{NaO}_3\text{S}$, 348 g/mol) is an anionic surfactant with a sulfonate headgroup, whereas Tween 80 ($\text{C}_{32}\text{H}_{60}\text{O}_{10}$, 605 g/mol) is a nonionic surfactant. All of the solutions and suspensions were prepared with deionized water. Pentafluorobenzoic acid (PFBA), purchased from Strem Chemicals (99%, Newburyport, MA), was used as a nonreactive tracer.

Two porous media were used for the column experiments. One is well sorted, 20/30 mesh sand (Accusand) purchased from Unimin Corporation. The other is Vinton soil (sandy, mixed, thermic Typic Torrifuvent), collected from the Ap horizon at the West Campus Agricultural Center in Tucson, Arizona. Properties of the media are presented in Table 1.

The columns used for the experiments are constructed of acrylic, and are 15 cm long and 2.6 cm in diameter. FMI Q type pumps (Fluid Metering, Inc.) were used to provide constant flow rates. Effluent samples were collected continuously in glass test tubes (for PFBA) or polypropylene test tubes (for PFOS) placed in a fraction collector (RediFrac, Pharmacia LKB).

2.2. Preparation of Suspensions

1 g of surfactant was dissolved in water and decanted into a 2 L volumetric flask to prepare a 500 mg/L surfactant solution. Then 50 mg of graphene nanoparticles was added to this 1L-surfactant solution to obtain a 50 mg/L graphene suspension. The graphene suspension was sonicated for 2.5 h to disperse the graphene nanoparticles. After that, the suspension was allocated into centrifuge tubes and centrifuged at 500 rpm for 90 min. After standing quiescent for 28 h, the supernatant from each centrifuge tube was collected with a syringe. The concentration of graphene was determined to be 2 mg/L by weighing the graphene remaining after supernatant collection. Graphene oxide suspensions were created in a similar manner, in the presence and absence of SDBS. The Z-average mean (cumulants mean) diameter and zeta potential of the colloidal particles were measured at the beginning and the end of the transport experiments by dynamic light scattering and electrophoretic light scattering, respectively, with a Zetasizer Nano (Malvern Instruments, UK).

2.3. Column Experiments

The column was dry packed with porous media, then deaired nanopure water was injected into the column at a slow flow rate until the porous medium was saturated. The column was weighed without soil, with dry soil, and with water-saturated soil, respectively, to determine water content and porosity. A nonreactive tracer test using PFBA was conducted for each new packed column to characterize hydrodynamic conditions.

Surfactant solution, with no graphene/graphene-oxide, was injected into the water-saturated column for 10 PVs. Approximately 4 PVs of surfactant-dispersed graphene/graphene-oxide suspension was then injected into the column. Unless otherwise specified, a flow rate of 1 mL/min was used, which is equivalent to a mean pore-water velocity of ~30 cm/h. The surfactant solution was then injected again into the column. Effluent samples were collected with the fraction collector, and analyzed with UV-vis spectrophotometry at 430 nm (SDBS-graphene) and 226 nm (Tween 80-graphene). The different conditions for the experiments are presented in Table 2.

2.4. Data Analysis

Breakthrough curves were obtained by plotting relative concentrations of the analyte in the effluent samples as a function of number of pore volumes eluted. Recoveries were determined by calculating the zeroth moment (area under the breakthrough curves), and mass balance was calculated as the quotient of the zeroth moment and the input quantity. Attachment efficiency coefficients (α), denoting the probability of attachment caused by the contacts between two surfaces (a suspended particle with another particle or with the filter), were calculated with the standard colloid filtration theory:

$$\ln \frac{C}{C_0} = -\frac{3}{2}(1-n)\alpha\eta \frac{L}{d_c}$$

where C and C_0 are effluent and influent concentration, n is porosity, L is the length of the packed column, d_c is the mean diameter of the collector (grain), and η is the single-collector efficiency, which comprises three components representing diffusion, interception, and sedimentation. Levich (1962) and Yao et al. (1971) obtained the analytical results for each of them: $\eta = \eta_D + \eta_I + \eta_G$

$$\eta_D = 0.9 \left(\frac{kT}{\mu d_p d_c v} \right)^{\frac{2}{3}}$$

$$\eta_I = \frac{3}{2} \left(\frac{d_p}{d_c} \right)^2$$

$$\eta_G = \frac{(\rho_p - \rho) g d_p^2}{18 \mu v}$$

k – Boltzmann's constant

T – absolute temperature

μ – water viscosity

d_p – diameter of the suspended particles

d_c – diameter of the collector

v – pore water velocity

ρ_p – density of the suspended particles

ρ – density of water

g – gravitational acceleration

3. Results and Discussion

The properties of surfactant-dispersed graphene suspension, measured by zetasizer, are listed in Table 3. The measured sizes of the surfactant-suspended graphene are consistent with the nominal lateral sizes provided by the manufacturer. It is observed that the diameters for tween-dispersed graphene are ~10% larger than those of the SDBS-graphene. This is most likely a result of greater compression of the electric double layer for the SDBS system and a much larger size of Tween 80 molecule than SDBS. The zeta potential for SDBS-graphene is substantially more negative than the Tween-graphene. This is because the negative charge on SDBS-graphene comes from the dissociation of SDBS molecules (negatively charged sulfonate headgroup) whereas the Tween 80-graphene's comes from shifting of the electron pair in a hydroxyl and the adsorption of anions around. The mean diameter of the colloidal particles increased by less than 3% and zeta potential increased by approximately 10-20% between the start and end of the experiments. The concentration of the graphene in reservoir was also measured at least three times at different phases of the experiments. The results show that there was minimal change during the course of the experiment and that the suspensions were stable.

The breakthrough curves for the nonreactive tracer, PFBA are sharp and symmetrical. Breakthrough occurred at 1 PV. Mass recoveries were > 99%. These results indicate that the columns were packed homogeneously and that hydrodynamic conditions were ideal.

The breakthrough curve for SDBS in sand is similar to that of the nonreactive tracer, indicating negligible retention and no retardation (see Figure 1). Minimal adsorption of SDBS by the sand is consistent with its geochemical properties (minimal organic carbon

and metal-oxides, no clay minerals). SDBS transport in Vinton soil is retarded, with a retardation factor of 3.8 and no irreversible retention (see Table 4). The greater adsorption of SDBS for Vinton is consistent with the presence of greater amounts of clay minerals, metal oxides, and organic carbon for Vinton versus the sand. Adsorption of Tween 80 on sand was estimated using Langmuir isotherm and parameters obtained from a reported batch experiment (Kang et al., 2015). The distribution coefficient, K_d , is approximately 5.6 mL/g. Based on this, it is anticipated that Tween 80 would have greater adsorption than SDBS.

Breakthrough curves for transport of graphene in sand and Vinton soil at different flow rates are shown in Figure 2-3. The breakthrough occurred at 1 PV for all experiments. Effluent concentrations exhibit plateaus at values less than the injection concentration, indicative of irreversible retention. The recoveries for graphene range from 50-86%, also indicating irreversible retention. These results are consistent with the standard transport behavior of colloids in porous media.

All of the graphene breakthrough curves displayed a slowly increasing relative-concentration plateau. This behavior is likely caused by the colloid blocking phenomenon. Initially, the media solids act as clean collectors devoid of colloid, and colloid deposition is maximized. As the surfaces of the solids become partially covered with colloid, attachment potential for incoming colloids is reduced (Dąbroś et al., 1982; Camesano et al., 1999). This results in an increase in the effluent concentration over time.

The recovery of SDBS-graphene (50%, see Table 5) is less than that of Tween 80-graphene (86%) for transport in the sand at a similar flow rate (~30 cm/h). Thus, SDBS-graphene experienced greater retention. Studies using molecular dynamics (MD)

simulations and experimental measurements have described the surface morphology of the surfactant-graphene assembly. Lin et al. (2011) observed that the hydrophobic tails of sodium cholate (SC, an anionic surfactant) are adsorbed onto the surface of graphene with a perpendicular orientation, with the hydrophilic heads directed away from the graphene surface into the bulk suspension. Arunachalam et al. (2017) proposed that the hydrophobic chains of cetyltrimethylammonium bromide (CTAB, a cationic surfactant) are weakly adsorbed to the graphene surface while exchanging rapidly with the free surfactants in the suspension. Therefore, graphene obtains an effective surface charge by the adsorption of ionic surfactants. Adsorbed ionic surfactants can increase the zeta potential of colloids and decrease the van der Waals force between the colloid and the solid surface and thus reduce the deposition (Batra et al., 2001).

As the sand surface is net-negatively charged, deposition should be more unfavorable for the likewise negatively charged SDBS-graphene, which conflicts with the observed result. However, studies investigating the stability and deposition of surfactant-dispersed colloid indicate the type and concentration of the surfactant, and ionic strength (IS) all play an important role in the deposition of surfactant-dispersed graphene. Du et al. (2013) proposed the addition of a nonionic surfactant, Triton X-100, can decrease colloid attachment by adsorbing onto both colloidal and collector surfaces and displacing the counterions to increase steric repulsion and expand the electric double layer, and the effect increases with increasing concentration of the surfactant. Zhuang et al. (2010) found that decreasing solution surface tension and IS can decrease colloid deposition and increase colloid recovery. But the two factors interact with each other. The effect of solution surface tension is greater at lower IS. Fan et al. (2015) conducted graphene oxide transport

experiments with SDBS and Triton X-100 under different IS and found that graphene oxide was more mobile at lower IS. And SDBS was more effective than Triton X-100 to facilitate graphene oxide transport. Poorsargol et al. (2019) reported sodium dodecyl sulfate (SDS, an anionic surfactant) was more effective than CTAB to disperse and stabilize graphene. They attributed this to the shorter tail and smaller head of SDS, which reduced the repulsive force between the SDS molecules and resulted in more adsorption of SDS on the graphene surface.

The lower recovery of SDBS-graphene (i.e., the greater retention) observed in the present study may be caused by excess SDBS ions in the bulk suspension, which increased the IS of the solution and compressed the double layer of the SDBS-graphene surface, making it more favorable to deposit onto the sand surface. Liu et al. (2015) reported an approximately 14% less recovery of SDBS-graphene at the SDBS concentration of 4000 mg/L compared with 40 mg/L.

There is more retention at 5 cm/h than at 27 cm/h for Tween 80-graphene transport in both media (Table 2). This is reasonable as a lower velocity reflects a larger residence time. A greater residence time provides more opportunity for the colloids to interact with the solid surfaces. The variation in retention at different flow velocities suggests that physical straining has minimal impact on retention. The ratio between the lateral size of graphene and the mean sand diameter is less than 0.02, which also indicates that physical straining is likely insignificant for retention.

For Tween 80-graphene at 5 cm/h and at 27 cm/h, there is more retention in Vinton soil than in sand. Vinton soil contains more organic carbon and metal oxides compared to the sand (Table 1). The pH of the solution used in this study is ~7.5, which is higher than

the point of zero charge (PZC) for iron oxide (5.9-7.1) but lower than that of aluminum oxide (8.5-9.4) (Kosmulski, 2018). Given the relative amount of the metal oxides Vinton soil contains, the impact of aluminum would be larger. Therefore, the metal oxide on soil surface is net positively charged, which is favorable for the deposition of tween 80-graphene. Besides, several studies have reported the enhancement of colloid deposition by metal hydr(oxide). Truesdail et al. (1998) investigated the deposition of four bacteria on aluminum and/or iron hydr(oxide) coated-sand vs untreated Ottawa sand and found the metal hydr(oxide)-coated sand increased the deposition of the bacteria by up to 5 times relative to untreated sand. Iron oxide or aluminum oxide-coated sand has also been reported to enhance the deposition of carboxymethyl cellulose (CMC) stabilized zero-valent iron (ZVI) nanoparticles (Zhang et al., 2017). Qi et al. (2019) found iron oxide-coated sand increased the deposition of graphene oxide nanoparticles by increasing the electrostatic attraction between the nanoparticles and sand surface, and by increasing sand surface roughness. Santamaria et al. (2012) conducted experiments to investigate transport of *Cryptosporidium Parvum* Oocysts in the same sand and Vinton soil as used in the present study. They observed greater retention in the Vinton soil compared to the sand, similar to as observed herein.

The breakthrough curve for graphene oxide transport in the sand, with no surfactant present, has a sharp arrival and elution wave, with a flat plateau equal to 1 (Figure 4 (A)). The recovery was essentially 100%, indicating no measurable retention. Graphene oxide has numerous hydroxyl, carboxyl, and epoxy groups on its surface and the edges. Once dispersed into water, they can remain stable without external intervention through

electrostatic repulsion. The presence of these functional groups likely minimize attachment at the sand surface.

To better compare the transport of graphene and graphene oxide, SDBS was added to the graphene oxide suspension for another experiment (Figure 4 (B)). The recovery of SDBS-graphene oxide was 83%, compared to 100% for no surfactant. Thus, the presence of SDBS is observed to cause some degree of retention of the graphene oxide. As discussed above, this may result from an increase of IS caused by the presence of SDBS in suspension.

The recovery of SDBS-graphene oxide is greater than that of SDBS-graphene (50%) in sand at 32 cm/h. Graphene oxide has a reported critical coagulation concentration (CCC) of 200 mmol/L NaCl (Chowdhury et al., 2015). Conversely, few-layer graphene has a CCC of 10 mmol/L NaCl (Su et al., 2017). Therefore, graphene is expected to agglomerate and have more retention than graphene oxide under the same conditions.

The attachment efficiencies calculated from the column experiments are reported in Table 5. They range from 10^{-4} to $4 * 10^{-3}$. To our knowledge these represent the first such values reported for graphene transport. Values in the range of $3 * 10^{-2}$ to 1 have been reported for graphene oxide and values of $8 * 10^{-3}$ to 1 and 10^{-2} to 1 have been reported for fullerene and single-walled/multi-walled carbon nanotubes in prior studies (Lecoanet et al., 2004; Jaisi et al., 2008; Mattison et al., 2011).

The attachment efficiencies calculated from the column experiments increased with increasing flow rate (Table 5). According to colloid filtration theory, the increase of flow velocity does not influence attachment efficiency (Ryan and Elimelech, 1996). Based on model simulations, Shen et al. (2010) predicted that the attachment efficiency does not

change with increasing flow velocity over a certain range, but will start decreasing once the flow velocity reaches a critical value. Apparent relationship between attachment efficiency and pore-water velocity have been observed in prior experiments. Lecoanet et al. (2004) reported increasing attachment efficiency with increasing flow velocity for fullerene at a high flow velocity. Zhang et al. (2018) observed a similar pattern for graphene oxide transport. Although the mechanisms still remain unclear, several studies have shown that the shape and size of colloid can affect the hydrodynamic forces exerted on the colloid and hence the attachment efficiency (Ryan and Elimelech, 1996; Salerno et al., 2006; Seymour et al., 2013). This may be a reason why an apparent velocity dependency was observed for the carbon nanoparticles such as fullerene, graphene oxide, and graphene.

4. Conclusion

Pore-water velocity, porous media geochemical properties, and surfactant type all have an effect on the transport of surfactant-dispersed graphene in porous media. More retention occurred at lower velocity and in the Vinton soil, which has higher amounts of organic matter and metal oxide. The anionic surfactant SDBS had no sorption for the sand but did for the Vinton soil. When added into the graphene suspension, it helped disperse and stabilize the graphene nanoparticles. The excess surfactant may also affect the solution chemistry and increase the deposition of graphene. All of the graphene breakthrough curves displayed an increasing concentration plateau, which can be explained as the existence of a colloid blocking effect. Overall, the results indicate graphene has some potential for transport in porous media. The migration potential is likely to be sensitive to solution chemistry and geochemical properties of the media.

Acknowledgements

This research was supported by the NIEHS Superfund Research Program (grant# P42 ES04940).

References

- ARUNACHALAM, V. & VASUDEVAN, S. 2017. Probing Graphene-Surfactant Interactions in Aqueous Dispersions with Nuclear Overhauser Effect NMR Spectroscopy and Molecular Dynamics Simulations. *Journal of Physical Chemistry C*, 121, 16637-16643.
- BAE, S., KIM, H., LEE, Y., XU, X. F., PARK, J. S., ZHENG, Y., BALAKRISHNAN, J., LEI, T., KIM, H. R., SONG, Y. I., KIM, Y. J., KIM, K. S., OZYILMAZ, B., AHN, J. H., HONG, B. H. & IIJIMA, S. 2010. Roll-to-roll production of 30-inch graphene films for transparent electrodes. *Nature Nanotechnology*, 5, 574-578.
- BAI, R. G., NINAN, N., MUTHOOSAMY, K. & MANICKAM, S. 2018. Graphene: A versatile platform for nanotheranostics and tissue engineering. *Progress in Materials Science*, 91, 24-69.
- BATRA, A., PARIA, S., MANOHAR, C. & KHILAR, K. C. 2001. Removal of surface adhered particles by surfactants and fluid motions. *Aiche Journal*, 47, 2557-2565.
- BLAKE, P., BRIMICOMBE, P. D., NAIR, R. R., BOOTH, T. J., JIANG, D., SCHEDIN, F., PONOMARENKO, L. A., MOROZOV, S. V., GLEESON, H. F., HILL, E. W., GEIM, A. K. & NOVOSELOV, K. S. 2008. Graphene-based liquid crystal device. *Nano Letters*, 8, 1704-1708.
- CAMESANO, T. A., UNICE, K. M. & LOGAN, B. E. 1999. Blocking and ripening of colloids in porous media and their implications for bacterial transport. *Colloids and Surfaces a-Physicochemical and Engineering Aspects*, 160, 291-308.
- CHENG, Z. G., LI, Q., LI, Z. J., ZHOU, Q. Y. & FANG, Y. 2010. Suspended Graphene Sensors with Improved Signal and Reduced Noise. *Nano Letters*, 10, 1864-1868.
- CHOWDHURY, I., MANSUKHANI, N. D., GUINEY, L. M., HERSAM, M. C. & BOUCHARD, D. 2015. Aggregation and Stability of Reduced Graphene Oxide:

- Complex Roles of Divalent Cations, pH, and Natural Organic Matter. *Environmental Science & Technology*, 49, 10886-10893.
- DABROS, T. & VANDEVEN, T. G. M. 1982. KINETICS OF COATING BY COLLOIDAL PARTICLES. *Journal of Colloid and Interface Science*, 89, 232-244.
- DU, Y. C., SHEN, C. Y., ZHANG, H. Y. & HUANG, Y. F. 2013. Effects of Flow Velocity and Nonionic Surfactant on Colloid Straining in Saturated Porous Media Under Unfavorable Conditions. *Transport in Porous Media*, 98, 193-208.
- FAN, W., JIANG, X. H., LU, Y., HUO, M. X., LIN, S. S. & GENG, Z. 2015a. Effects of surfactants on graphene oxide nanoparticles transport in saturated porous media. *Journal of Environmental Sciences*, 35, 12-19.
- FAN, W., JIANG, X. H., YANG, W., GENG, Z., HUO, M. X., LIU, Z. M. & ZHOU, H. 2015b. Transport of graphene oxide in saturated porous media: Effect of cation composition in mixed Na-Ca electrolyte systems. *Science of the Total Environment*, 511, 509-515.
- HERNANDEZ, Y., NICOLOSI, V., LOTYA, M., BLIGHE, F. M., SUN, Z. Y., DE, S., MCGOVERN, I. T., HOLLAND, B., BYRNE, M., GUN'KO, Y. K., BOLAND, J. J., NIRAJ, P., DUESBERG, G., KRISHNAMURTHY, S., GOODHUE, R., HUTCHISON, J., SCARDACI, V., FERRARI, A. C. & COLEMAN, J. N. 2008. High-yield production of graphene by liquid-phase exfoliation of graphite. *Nature Nanotechnology*, 3, 563-568.
- JAISI, D. P., SALEH, N. B., BLAKE, R. E. & ELIMELECH, M. 2008. Transport of Single-Walled Carbon Nanotubes in Porous Media: Filtration Mechanisms and Reversibility. *Environmental Science & Technology*, 42, 8317-8323.
- KANG, S. & JEONG, H. Y. 2015. Sorption of a nonionic surfactant Tween 80 by minerals and soils. *Journal of Hazardous Materials*, 284, 143-150.
- KOSMULSKI, M. 2018. The pH dependent surface charging and points of zero charge. VII. Update. *Advances in Colloid and Interface Science*, 251, 115-138.
- LANPHERE, J. D., LUTH, C. J. & WALKER, S. L. 2013. Effects of Solution Chemistry on the Transport of Graphene Oxide in Saturated Porous Media. *Environmental Science & Technology*, 47, 4255-4261.

- LECOANET, H. F. & WIESNER, M. R. 2004. Velocity effects on fullerene and oxide nanoparticle deposition in porous media. *Environmental Science & Technology*, 38, 4377-4382.
- LEVICH, V. 1962. *Physicochemical hydrodynamics*, pp.80-85.
- LI, X. M., TAO, L., CHEN, Z. F., FANG, H., LI, X. S., WANG, X. R., XU, J. B. & ZHU, H. W. 2017. Graphene and related two-dimensional materials: Structure-property relationships for electronics and optoelectronics. *Applied Physics Reviews*, 4, 31.
- LI, X. S., CAI, W. W., AN, J. H., KIM, S., NAH, J., YANG, D. X., PINER, R., VELAMAKANNI, A., JUNG, I., TUTUC, E., BANERJEE, S. K., COLOMBO, L. & RUOFF, R. S. 2009. Large-Area Synthesis of High-Quality and Uniform Graphene Films on Copper Foils. *Science*, 324, 1312-1314.
- LIN, S. C., SHIH, C. J., STRANO, M. S. & BLANKSCHTEIN, D. 2011. Molecular Insights into the Surface Morphology, Layering Structure, and Aggregation Kinetics of Surfactant-Stabilized Graphene Dispersions. *Journal of the American Chemical Society*, 133, 12810-12823.
- LIU, L., GAO, B., WU, L., MORALES, V. L., YANG, L. Y., ZHOU, Z. H. & WANG, H. 2013. Deposition and transport of graphene oxide in saturated and unsaturated porous media. *Chemical Engineering Journal*, 229, 444-449.
- LIU, L., GAO, B., WU, L., SUN, Y. Y. & ZHOU, Z. H. 2015. Effects of surfactant type and concentration on graphene retention and transport in saturated porous media. *Chemical Engineering Journal*, 262, 1187-1191.
- MATTISON, N. T., O'CARROLL, D. M., ROWE, R. K. & PETERSEN, E. J. 2011. Impact of Porous Media Grain Size on the Transport of Multi-walled Carbon Nanotubes. *Environmental Science & Technology*, 45, 9765-9775.
- NI, Z. H., WANG, H. M., KASIM, J., FAN, H. M., YU, T., WU, Y. H., FENG, Y. P. & SHEN, Z. X. 2007. Graphene thickness determination using reflection and contrast spectroscopy. *Nano Letters*, 7, 2758-2763.
- NOVOSELOV, K. S., FAL'KO, V. I., COLOMBO, L., GELLERT, P. R., SCHWAB, M. G. & KIM, K. 2012. A roadmap for graphene. *Nature*, 490, 192-200.

- POORSARGOL, M., ALIMOHAMMADIAN, M., SOHRABI, B. & DEHESTANI, M. 2019. Dispersion of graphene using surfactant mixtures: Experimental and molecular dynamics simulation studies. *Applied Surface Science*, 464, 440-450.
- QI, Z. C., DU, T. T., MA, P. K., LIU, F. F. & CHEN, W. 2019. Transport of graphene oxide in saturated quartz sand containing iron oxides. *Science of the Total Environment*, 657, 1450-1459.
- QI, Z. C., ZHANG, L. L., WANG, F., HOU, L. & CHEN, W. 2014. FACTORS CONTROLLING TRANSPORT OF GRAPHENE OXIDE NANOPARTICLES IN SATURATED SAND COLUMNS. *Environmental Toxicology and Chemistry*, 33, 998-1004.
- REN, W. C. & CHENG, H. M. 2014. The global growth of graphene. *Nature Nanotechnology*, 9, 726-730.
- RYAN, J. N. & ELIMELECH, M. 1996. Colloid mobilization and transport in groundwater. *Colloids and Surfaces a-Physicochemical and Engineering Aspects*, 107, 1-56.
- SALERNO, M. B., FLAMM, M., LOGAN, B. E. & VELEGOL, D. 2006. Transport of rodlike colloids through packed beds. *Environmental Science & Technology*, 40, 6336-6340.
- SANTAMARIA, J., BRUSSEAU, M. L., ARAUJO, J., OROSZ-COGLAN, P., BLANFORD, W. J. & GERBA, C. P. 2012. Transport and Retention of *Cryptosporidium Parvum* Oocysts in Sandy Soils. *Journal of Environmental Quality*, 41, 1246-1252.
- SASIDHARAN, A., PANCHAKARLA, L. S., CHANDRAN, P., MENON, D., NAIR, S., RAO, C. N. R. & KOYAKUTTY, M. 2011. Differential nano-bio interactions and toxicity effects of pristine versus functionalized graphene. *Nanoscale*, 3, 2461-2464.
- SAWOSZ, E., JAWORSKI, S., KUTWIN, M., HOTOWY, A., WIERZBICKI, M., GRODZIK, M., KURANTOWICZ, N., STROJNY, B., LIPINSKA, L. & CHWALIBOG, A. 2014. Toxicity of pristine graphene in experiments in a chicken embryo model. *International Journal of Nanomedicine*, 9, 3913-3922.

- SEYMOUR, M. B., CHEN, G. X., SU, C. M. & LI, Y. S. 2013. Transport and Retention of Colloids in Porous Media: Does Shape Really Matter? *Environmental Science & Technology*, 47, 8391-8398.
- SHEN, C. Y., HUANG, Y. F., LI, B. G. & JIN, Y. 2010. Predicting attachment efficiency of colloid deposition under unfavorable attachment conditions. *Water Resources Research*, 46, 12.
- SU, Y., GAO, B. & MAO, L. 2017. Concurrent agglomeration and straining govern the transport of C-14-labeled few-layer graphene in saturated porous media. *Water Research*, 115, 84-93.
- SUN, Y. Y., GAO, B., BRADFORD, S. A., WU, L., CHEN, H., SHI, X. Q. & WU, J. C. 2015. Transport, retention, and size perturbation of graphene oxide in saturated porous media: Effects of input concentration and grain size. *Water Research*, 68, 24-33.
- THE ROYAL SWEDISH ACADEMY OF SCIENCES. 2010. Scientific Background on the Nobel Prize in Physics.
- TRUESDAIL, S. E., LUKASIK, J., FARRAH, S. R., SHAH, D. O. & DICKINSON, R. B. 1998. Analysis of bacterial deposition on metal (hydr)oxide-coated sand filter media. *Journal of Colloid and Interface Science*, 203, 369-378.
- YAO, K. M., HABIBIAN, M. M. & OMELIA, C. R. 1971. WATER AND WASTE WATER FILTRATION - CONCEPTS AND APPLICATIONS. *Environmental Science & Technology*, 5, 1105-&.
- YIN, X. Q., JIANG, Y. J., TAN, Y. H., MENG, X. M., SUN, H. M. & WANG, N. 2019. Co-transport of graphene oxide and heavy metal ions in surface-modified porous media. *Chemosphere*, 218, 1-13.
- ZHANG, C. L., YAN, A., WANG, G., JIN, C., CHEN, Y. H. & SHEN, C. Y. 2018. Impact of Flow Velocity on Transport of Graphene Oxide Nanoparticles in Saturated Porous Media. *Vadose Zone Journal*, 17, 10.
- ZHANG, M., HE, F., ZHAO, D. Y. & HAO, X. D. 2017. Transport of stabilized iron nanoparticles in porous media: Effects of surface and solution chemistry and role of adsorption. *Journal of Hazardous Materials*, 322, 284-291.

ZHU, Y. W., MURALI, S., CAI, W. W., LI, X. S., SUK, J. W., POTTS, J. R. & RUOFF, R. S. 2010. Graphene and Graphene Oxide: Synthesis, Properties, and Applications. *Advanced Materials*, 22, 3906-3924.

ZHUANG, J., GOEPPERT, N., TU, C., MCCARTHY, J., PERFECT, E. & MCKAY, L. 2010. Colloid transport with wetting fronts: Interactive effects of solution surface tension and ionic strength. *Water Research*, 44, 1270-1278.

Table 1. Properties of porous media.

Porous Media	SSA¹ (m² g⁻¹)	Median Grain Diameter (mm)	Zeta Potential (mV)	Clay (%)	TOC	Fe (µg g⁻¹)	Al (µg g⁻¹)	Mn (µg g⁻¹)
Accusand 20/30	0.137	0.71	-51.2±12	0	0.04	14	12	2.5
Vinton soil	3.54	0.26	-38.9±6	1.2	0.1	1700	1400	130

¹Solid surface area measured by N₂/BET

Table 2. Experiment conditions.

Porous media	nanoparticle	Surfactant	Porosity	v cm h⁻¹	Bulk density g cm⁻³	C₀ mg L⁻¹
Sand	graphene	SDBS	0.3528	32	1.76	2
Sand	graphene	Tween 80	0.3566	5	1.74	2
Sand	graphene	Tween 80	0.3717	27	1.73	2
Vinton	graphene	Tween 80	0.4596	5	1.57	2
Vinton	graphene	Tween 80	0.4244	27	1.53	2
Sand	Graphene oxide	none	0.3328	34	1.61	5
Sand	Graphene oxide	SDBS	0.3478	32	1.70	5

Table 3. Properties of the graphene suspensions.

Sample	Mean Diameter (d.nm)	Zeta Potential (mV)
Tween 80-graphene_start	2978	-22.7
Tween 80-graphene_end	3045	-25.1
SDBS-graphene_start	2669	-44.9
SDBS-graphene_end	2697	-54.2

Table 4. Results for SDBS (only) transport in sand and Vinton soil.

Porous Media	v (cm/h)	Recovery (%)	Retardation factor	K_d (mL/g)
Sand	32	107	1	0
Vinton	8	100	3.8	0.64

Table 5. Recoveries and attachment efficiencies for each experiment.

Porous media	nanoparticle	Surfactant	v (cm/h)	Recovery (%)	Attachment Efficiency
Sand	graphene	Tween 80	5	82	0.0009
Sand	graphene	Tween 80	27	86	0.0038
Vinton	graphene	Tween 80	5	56	0.0011
Vinton	graphene	Tween 80	27	85	0.0016
Sand	graphene	SDBS	32	50	0.0019
Sand	Graphene oxide	SDBS	32	83	0.0052
Sand	Graphene oxide	none	34	107	0

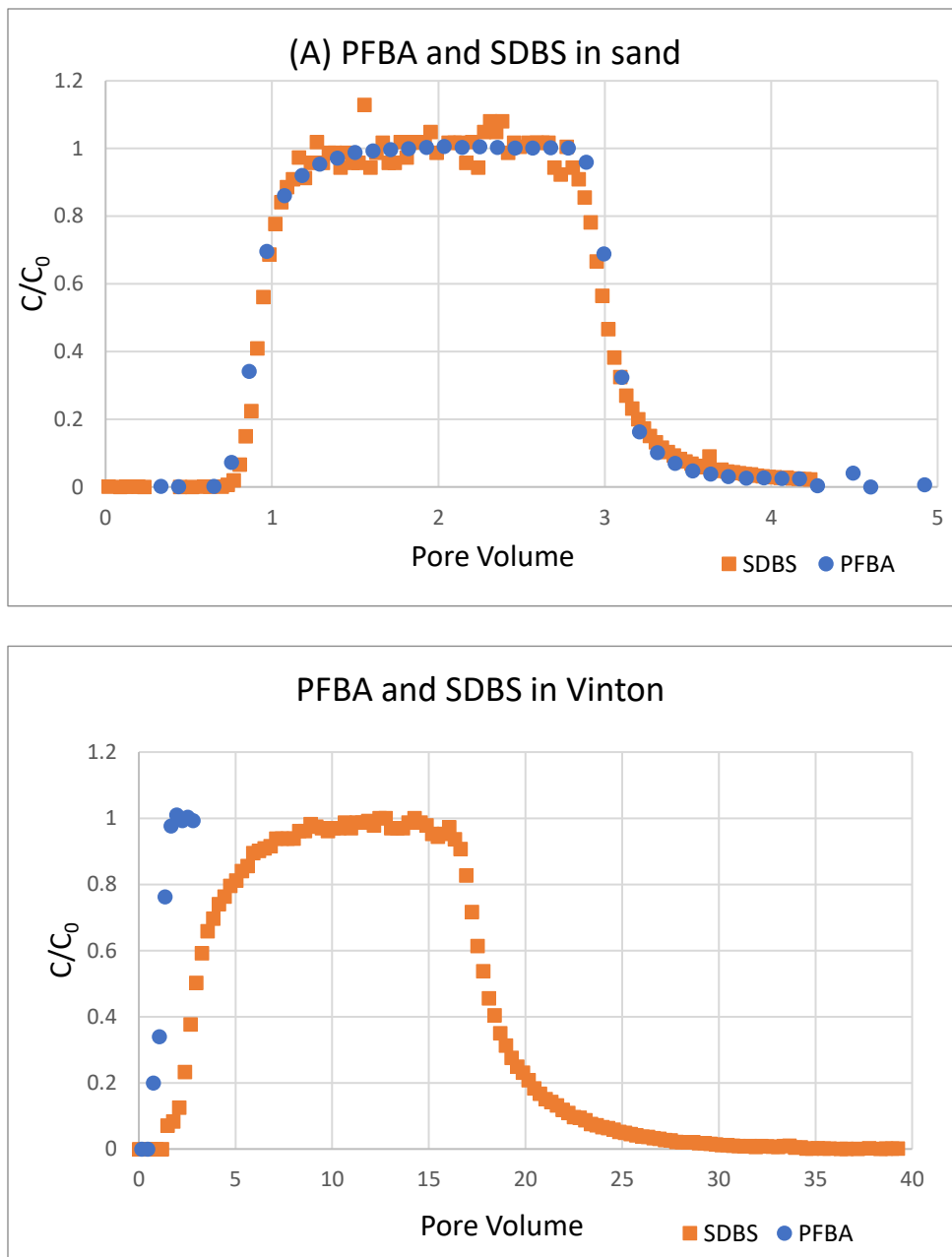


Figure 1. Breakthrough curves of PFBA and SDBS in (A) sand and (B) Vinton soil.

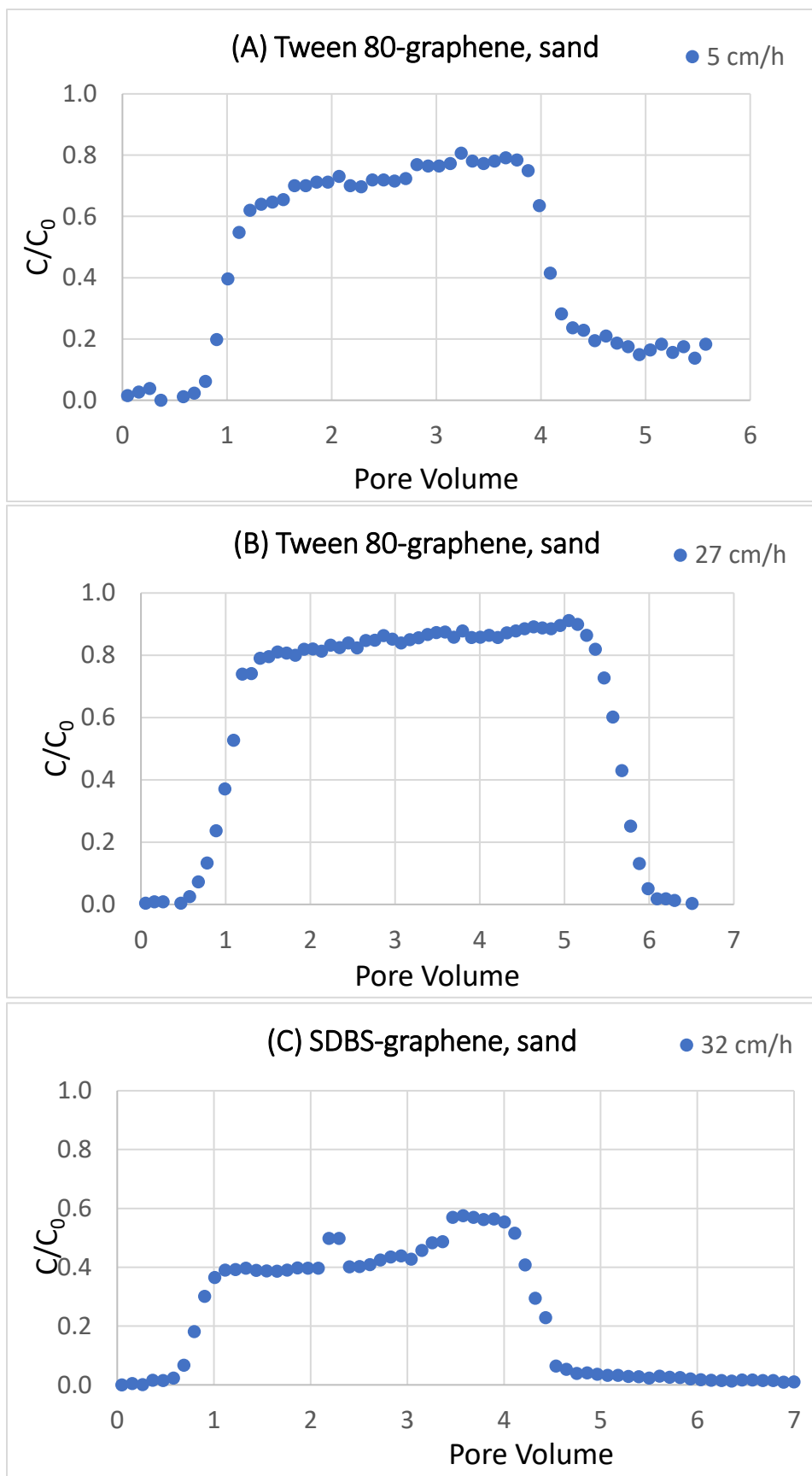


Figure 2 (A), (B), (C). Breakthrough curves for transport of surfactant-dispersed graphene in sand at different flow rates.

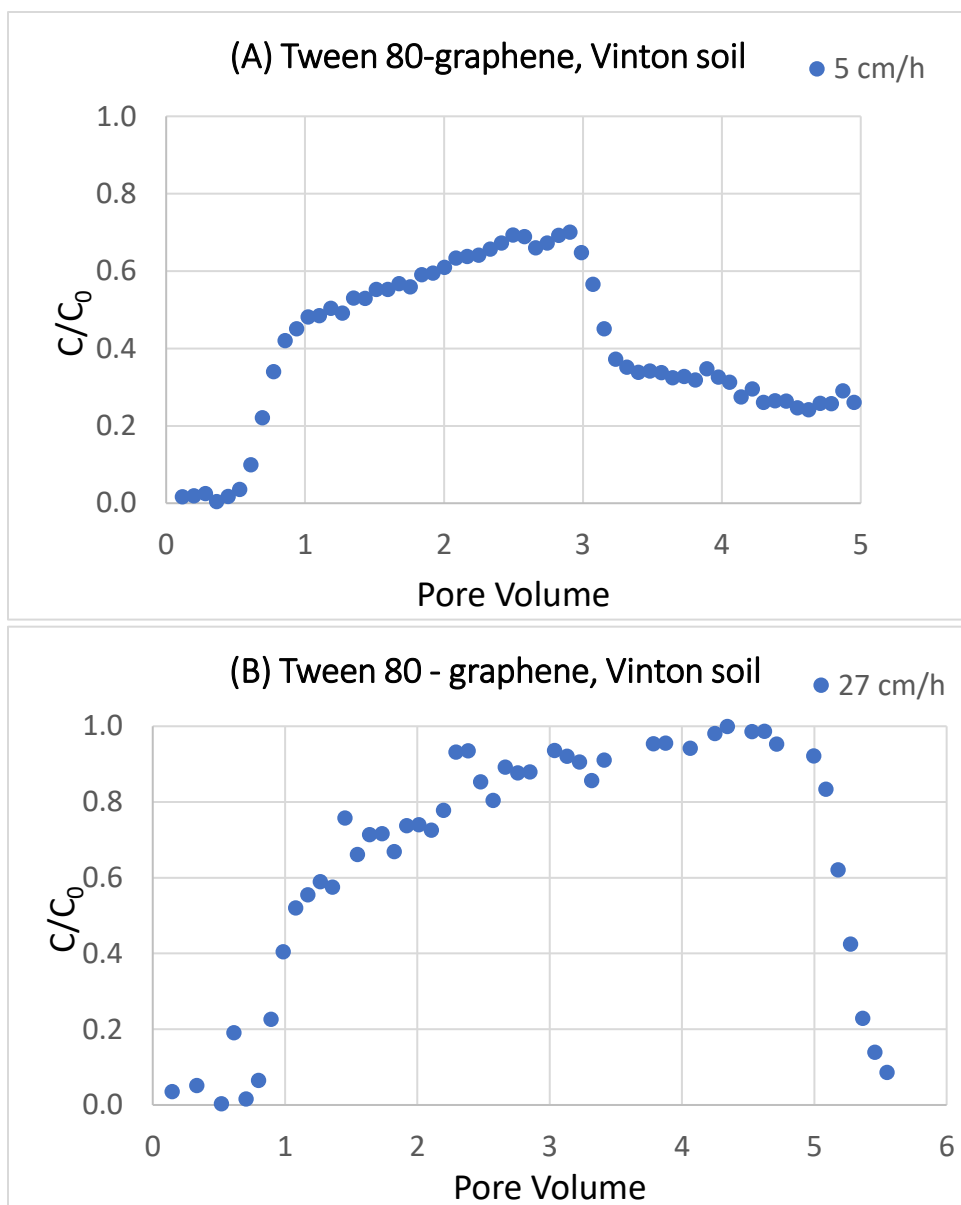


Figure 3 (A), (B). Breakthrough curves for transport of surfactant-dispersed graphene in Vinton soil at different flow rates.

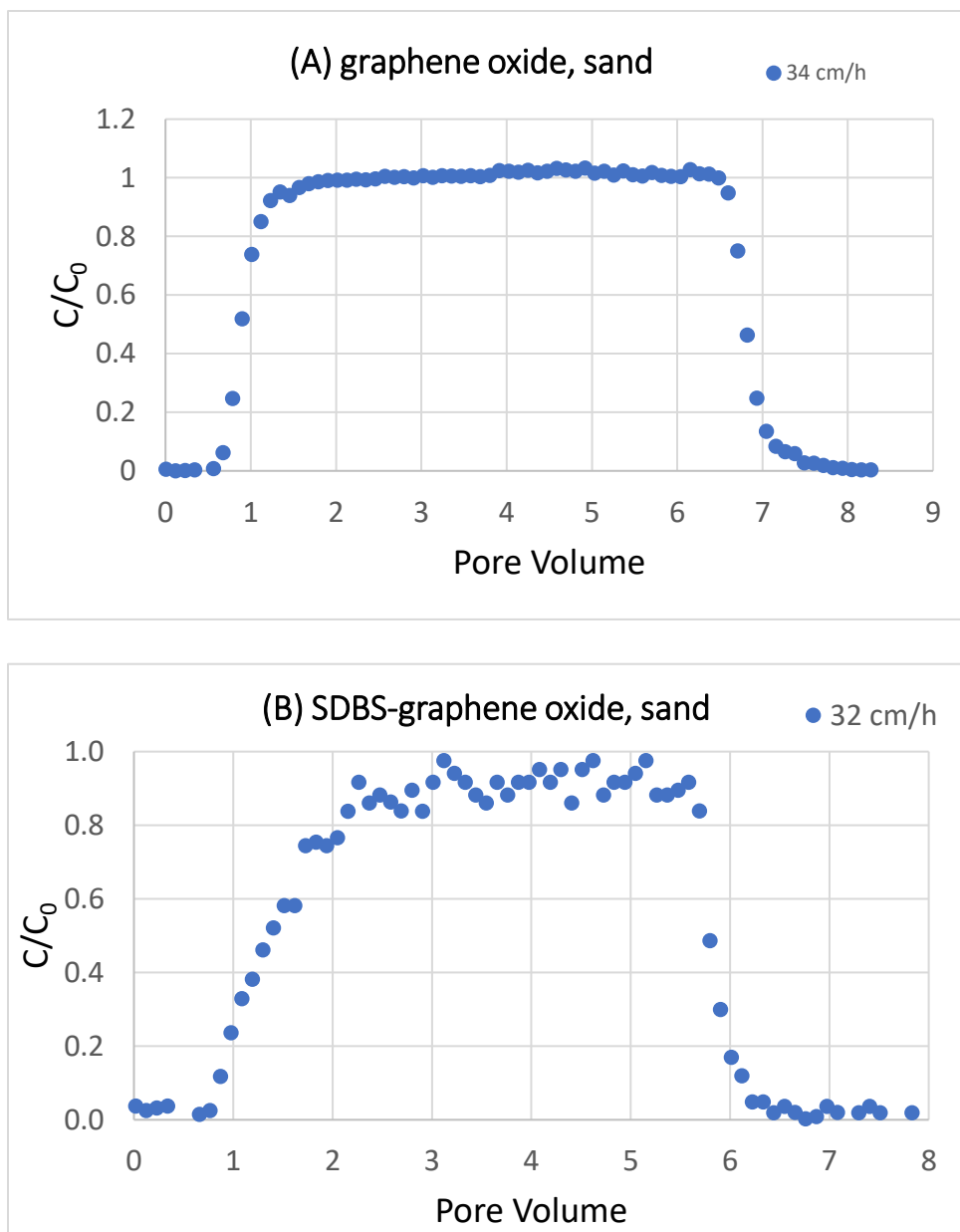


Figure 4 (A), (B). Breakthrough curves for transport of graphene oxide with or without SDBS in sand at ~ 30 cm/h.

**APPENDIX B – NONIDEAL TRANSPORT AND EXTENDED ELUTION
TAILING OF PFOS IN SOIL AND AQUIFER SEDIMENT**

Yake Wang

Co-authors: Naima Khan, Ni Yan, Kenneth C. Carroll, and Mark L. Brusseau*

*Corresponding author: Brusseau@email.arizona.edu

Abstract

The objective of this research was to examine the influence of nonideal sorption/desorption on the transport of PFAS in porous media, with a specific focus on characterizing and quantifying potential extended, mass-transfer-limited elution behavior. PFOS was used as a representative PFAS, and miscible-displacement experiments were conducted with two soils and three aquifer sediments comprising contrasting geochemical properties. The influence of nonlinear, rate-limited, hysteretic, and irreversible sorption/desorption on transport was investigated through experiments and model simulations. The breakthrough curves measured for PFOS transport were asymmetrical and exhibited extensive elution tailing, indicating that sorption/desorption was significantly nonideal. The widely used two-domain sorption-kinetics (TDSK) model could not fully simulate the observed transport behavior, whereas a multi-rate model employing a continuous distribution of sorption domains (CDMR) was successful. The overall results indicated that sorption/desorption was significantly rate-limited, and that nonlinear, hysteretic, and irreversible sorption/desorption had minimal impact on PFOS transport. Comparison of PFOS transport data to data reported for two hydrophobic organic contaminants (HOCs) showed that the HOCs exhibited much more extensive elution tailing, likely reflecting differences in sorption/desorption mechanisms. The projected influence of rate-limited sorption/desorption on PFOS transport at the field scale was investigated through simulation.

1. Introduction

Per- and polyfluoroalkyl substances (PFASs) have been detected in surface water, sediments, soils, groundwater and wastewater globally due to their widely use in fast food packages, non-stick coatings, fire-fighting foams in the past few decades (Zareitalabad et al., 2013). The hydrocarbon chains of PFAS molecules are highly or fully fluorinated. The strong carbon-fluorine bonds make PFAS nonbiodegradable and persistent in the environment (Key et al., 1997). Recently, the human health concern has also arisen as the toxicity and bioaccumulation of PFAS have been confirmed. USEPA (2016) established a lifetime health advisory level (HAL) of 70 ng/L for the combined concentrations of PFOS and PFOA, the most widely used and studied PFASs, in drinking water. The U.S. Agency for Toxic Substances and Disease Registry released a report last year suggesting levels should be in the range of ~20 ng/L (ASTDR, 2018). These risk levels are much lower than the maximum contaminant levels established for other common contaminants such as arsenic (10 µg/L) and trichloroethene (5 µg/L).

Understanding the transport and retention behavior would help evaluate the risks of PFAS contamination in groundwater and design effective remediation methods. However, until now, only limited studies on PFOS transport have been reported. McKenzie et al. (2015) investigated the transport of perfluorooctanoic acid (PFOA), perfluorooctane sulfonic acid (PFOS), and other PFAS in a loamy sand. Brusseau and colleagues (Lyu et al., 2018; Brusseau et al., 2019) investigated the transport of PFOA and PFOS in quartz sands and a soil. Lv et al. (2018) examined the transport of PFOA in quartz sand and in limestone. Aly et al. (2018) conducted column experiments to test the effect of two amendments to enhance sorption of PFOS onto quartz sand. The majority of the prior

research has focused on PFAS transport in ideal, geochemically simple porous media. It is anticipated that the magnitude and complexity of PFAS adsorption will be greater for transport in soils and aquifer materials. Investigating transport in more soils and aquifer materials would be helpful to study the more complicated retention mechanisms for PFOS transport in groundwater.

In this study, miscible-displacement experiments with two soils and three aquifer materials of different geochemical properties were conducted to investigate the transport and retention of PFOS. Some sets of experiments were treated with extended elution time to investigate the potential extensive elution tailing of breakthrough curves (BTCs) which reflects nonideal sorption/desorption. Two mathematical models incorporating different sorption/desorption kinetics were used to determine which one is the dominant factor.

2. Materials and Methods

2.1 Materials

Six porous media of similar median grain diameter but different geochemical properties were used--- Vinton soil, Eustis soil, Borden aquifer material, Hanford aquifer material, AFP 44 aquifer material, and commercial natural quartz sand. Select properties of the media are presented in Table 1. The Eustis soil (siliceous, thermic Psammentic Paleudults) is composed primarily of quartz, with small fractions of feldspar (0.5%) and clay minerals (1.7%, essentially all kaolinite). It has a total organic-carbon content of 0.38%, consisting of approximately 37% hard carbon (kerogen and black carbon) and 63% soft carbon (humic/fulvic acids, lipids). It has a relatively low metal-oxide content. The Vinton soil (sandy, mixed, thermic Typic Torrifluent) consists of 54% silica, 36%

feldspar, 3% amphibole, and 4.7% clay minerals. The clay minerals consist of similar proportions of kaolinite, vermiculite, and illite, with small fractions of montmorillonite and amorphous silica. It has a lower (0.1%) organic-carbon content and a higher metal-oxide content. The Borden medium was collected from the Canadian AFB Ontario, which is a well-known site for contaminant hydrology field studies. It has low organic carbon and oxide content. The Hanford medium was collected from the Hanford, WA Department of Energy facility. It has a quite high iron oxide content and low organic carbon. The AFP44 medium was collected from the AFP44 site, which is part of the Tucson International Airport Area Superfund site in Tucson, AZ. It has low organic carbon. A commercial natural quartz sand (Accusand, Unimin, Corp) was used as a reference medium. This material has low organic carbon and metal oxide contents, and no clay minerals.

PFOS (98%) was purchased from Sigma-Aldrich. Pentafluorobenzoic acid (PFBA) (99%, Strem Chemicals) was used as the nonreactive tracer. A synthetic groundwater was prepared by dissolving select salts into distilled, deionized water as the background electrolyte. Major ions are listed in Table 2. The pH and ionic strength (IS) are 7.7 and 0.01 M, respectively. 10 mg/L PFOS solutions were prepared for all the experiments. The columns used for the experiments are constructed of acrylic or stainless steel, with a length of 7-20 cm and an inner diameter of 2-2.5 cm.

2.2 Miscible-displacement Experiments

The columns were dry packed with the porous media uniformly and set vertically. Precision HPLC pumps were used to provide a constant flow rate of 1 mL/min, equivalent to a mean pore-water velocity of ~50 cm/h. Synthetic groundwater was first injected into

the column from the bottom at a very slow flow rate until saturation. Then the nonreactive tracer, PFBA (120 mg/L, dissolved in synthetic groundwater), was injected into the column for 3-4 PVs, followed by another ~10 PVs of synthetic groundwater. After this, ~20 PVs of PFOS solution (10 mg/L, dissolved in synthetic groundwater) was injected into the column, followed by another ~50 PVs of synthetic groundwater. Experiment sets conducted with such input time and elution time aimed to observe the potential extended elution tailing. Time setting varies in other standard miscible-displacement experiments.

2.3 Analytical Methods

The pentafluorobenzoic acid samples were analyzed by ultraviolet-visible (UV-Vis) spectrophotometry (Shimadzu, model 1601) at wavelengths of 262 and 226 nm, respectively. The quantitative detection limits (QDL) for UV-Vis is approximately 1 mg/L.

PFOS samples were analyzed by two methods. The first method employed the methylene blue active substances (MBAS) assay (Chitikela et al., 1995), and analyzed with UV-vis spectrophotometry at 650 nm. This is a standard method used to quantify anionic surfactant concentrations (ASTM D2330-02), and has been used successfully for PFAS analysis under conditions wherein a single PFAS is present (Brusseau et al., 2019). Detailed description of the method is provided in the references cited. The quantifiable detection limit is ~0.4 mg/L for PFOS.

The second method for PFOS analysis employed High Performance Liquid Chromatography tandem mass spectrometry (LCMS). The analysis employed a Waters Alliance 2695 LC coupled to a Micromass Quattro Ultima Triple Quadrupole MS system, using negative electrospray ionization (ESI-). A Thermoscientific Betasil™ C18, 2.1 ×

150mm, 5 μm particle size analytical column was used. Aqueous samples of 3 or 5 μL volume were injected directly. Elution was performed using two eluents, with a flow rate of 0.2 mL/min. Eluent A comprised water + 5 mM ammonium acetate while eluent B consisted of 90% acetonitrile + 10% water + 5 mM ammonium acetate. From 0 – 4.49 min, the solvent gradient was 80% A and 20% B. For 4.5 – 5 min, the solvent gradient was 4% A and 96% B. For 5 – 20 min, the solvent gradient was isocratic, comprising 100% B. The column was re-equilibrated for 15 min between samples at the initial conditions. The column temperature was maintained at 30 $^{\circ}\text{C}$.

Standard QA/QC protocols were employed. Blanks, background samples, and check standards were analyzed periodically for each sample set. The results for the first two were lower than the quantifiable detection limit. The coefficients of determination (r^2) for the calibration curves were larger than 0.99. The QDL is $\sim 0.2 \mu\text{g/L}$ for PFOS. Background aqueous samples collected from the column effluent before injection of PFOS revealed no measurable concentrations or other interferences for all experiments.

2.4 Simulation for the Experimental Data

Two solute-transport models were used to simulate the breakthrough curves obtained from the experiments. They are based on the one-dimensional advection-dispersion equation incorporating different sorption kinetics.

In two-domain sorption-kinetics (TDSK) model, sorption is assumed to reach equilibrium instantaneously for part of the domain and be rate-limited for the remaining domain. Herein Freundlich isotherm is used to describe the two-domain sorption/desorption:

$$S_1 = FK_f C^N$$

$$S_2 = (1 - F)K_f C^N$$

$$\frac{dS_2}{dt} = k_2[(1 - F)K_f C^N - S_2]$$

where C is solute concentration in solution ($M L^{-3}$), S_1 is solute concentration in sorbed phase for instantaneous domain ($M M^{-1}$), S_2 is solute concentration in sorbed phase in the rate-limited domain ($M M^{-1}$), K_f is Freundlich sorption coefficient ($L^{3N} M^{-N}$), N is Freundlich exponent, k_1 , k_2 are first-order adsorption, desorption rate coefficients (T^{-1}).

One-dimensional solute transport under steady state flow and nonlinear, rate-limited sorption with nondimensional terms can be described as follows:

$$(1 - \beta)R \frac{\partial S^*}{\partial T} = \omega(C^{*N} - S^*)$$

$$\frac{\partial C^*}{\partial T} + (\beta R - 1)NC^{*N-1} \frac{\partial C^*}{\partial T} + \omega(C^{*N} - S^*) = \frac{1}{P} \frac{\partial^2 C^*}{\partial X^2} - \frac{\partial C^*}{\partial X}$$

Each nondimensional term is defined by:

$$C^* = \frac{C}{C_0}$$

$$S^* = \frac{S_2}{(1 - F)K_f C_0^N}$$

$$T = \frac{vt}{L}$$

$$X = \frac{x}{L}$$

$$P = \frac{vL}{D}$$

$$\omega = \frac{k_2(1 - \beta)RL}{v}$$

$$R = 1 + \frac{\rho_b}{\theta_w} K_f C_0^{N-1}$$

$$\beta = \frac{1 + \frac{\rho_b}{\theta_w} FK_f C_0^{N-1}}{R}$$

where C_0 is solute input concentration ($M L^{-3}$), v is mean pore-water velocity ($L T^{-1}$), L is column length (L), x is distance (L), P is Peclet number, D is dispersion coefficient, ω is

Damkohler number, R is retardation factor, ρ_b is bulk density ($M L^{-3}$), θ_w is volumetric water content, β is fraction of retardation that is effectively instantaneous.

In continuous-distribution multi-rate (CDMR) model, first-order rate coefficient for the sorption/desorption kinetics, k_2 , is defined as a random variable with a ln-normal distribution (e.g., Johnson et al., 2003):

$$f(k_2) = \frac{1}{\sqrt{2\pi}k_2\sigma_k} \exp\left(-\frac{[\ln(k_2) - \mu]^2}{2\sigma_k^2}\right)$$

where μ is the mean of $\ln(k_2)$, σ_k is the variance of $\ln(k_2)$. Sorption for the equilibrium and rate-limited domains are described as:

$$\frac{\partial S_{eq}}{\partial t} = FK_f C^N \frac{\partial C}{\partial t}$$

$$\frac{\partial S_i}{\partial t} = k_{2i}[(1 - F)K_f C^N - S_i]$$

The advection-dispersion equation incorporating the sorption terms thus can be expressed as:

$$\frac{\partial C}{\partial t} + \frac{\rho_b}{\theta} \frac{\partial S_{eq}}{\partial t} + \frac{\rho_b}{\theta} \sum_{i=1}^m f_i(k_{2i}) \frac{\partial S_i}{\partial t} = -v \frac{\partial C}{\partial x} + D \frac{\partial^2 C}{\partial x^2}$$

where m is the total number of domains. A set of 100 has been proved to be sufficient to obtain effective distribution (Li et al., 2000; Schnaar et al., 2014).

3. Results and Discussion

The breakthrough curves for the nonreactive tracer were ideal, with sharp arrival and elution waves, and retardation factors of 1 (Figures 1 and 2), indicating that the porous media were homogeneously packed and water flow was uniform.

Standard miscible-displacement experiments for PFOS in Eustis and Vinton soils are presented in Figures 1 and 2. Prominent arrival-wave and elution-wave tailing were observed, reflecting the influence of nonideal (nonlinear/rate-limited/hysteretic) sorption/desorption on transport. The TDSK model provides good simulations. Figures 3 and 4 show the breakthrough curves for PFOS transport in Eustis and Vinton soils with extended time to specifically observe the elution tailings. Simulations provided by TDSK model cannot fit the tailing, while the CDMR model provides an excellent match.

PFOS recoveries are close to 100% for the extended experiments, indicating reversible sorption. The influence of nonlinear, rate-limited, hysteretic sorption/desorption on transport was examined by adjusting the combination of these processes in the simulations and finding out the optimal fit. It is found that the impact of nonlinear, hysteretic adsorption was very minor, while rate-limited adsorption was the primary cause of the observed nonideal transport.

Breakthrough curves for PFOS in three aquifer materials – Borden, AFP 44, Hanford are displayed in Figures 5-7. The simulations provided by TDSK model fit the bulk breakthrough curves well but deviate for the extended elution tailing.

Figure 8 presents a comparison of the extended elution tailing of PFOS in the six porous media with the pore volume (x-axis) normalized by the respective retardation factors of the compounds to eliminate the effect of differences in the magnitudes of retardation on the extents of tailing. PFOS has greater tailing in the two soils than in aquifer materials and sand. This is consistent with a prior study conducted by Brusseau and colleagues investigating the elution tailings of TCE in several soils and aquifer materials (Figure 9), some of which are the same with those used in this study. The fact that the

extent of retardation-normalized elution tailing does not correlate with the general magnitude of adsorption suggests the composition of the soil components may influence the sorption/desorption behavior (Russo et al., 2010).

In other prior miscible-displacement studies (Kempf and Brusseau, 2009; Schnaar and Brusseau, 2014), transport of several HOCs in the Eustis soil was investigated under extended time. Representative elution-wave data sets with normalized x-axis for trichloroethene (TCE) and atrazine are presented in Figure 10 for the Eustis soil, along with the PFOS and NRT data. The HOCs have much greater tailing compared to PFOS. It is noteworthy that the retardation factors for TCE and atrazine transport in the Eustis soil are 3 and 3.5, which are slightly smaller than that of PFOS. Hence, for similar magnitudes of sorption and retardation, TCE and atrazine exhibit much greater elution tailing compared to PFOS.

This significant difference in the magnitude of mass-transfer limitations likely reflects differences in the mechanisms mediating sorption/desorption of PFOS versus the HOCs. Prior research has demonstrated that the sorption/desorption of HOCs in the Eustis soil is controlled by adsorption to and permeation within the soil organic carbon. Conversely, adsorption of PFOS and other PFAS can be influenced significantly by surface interactions with metal oxides and clay minerals as well as interaction with organic carbon.

While the use of organic-carbon normalized adsorption coefficients (K_{oc}) is uncertain for PFAS, they can be calculated to help illuminate potential adsorption mechanisms. Log K_{oc} values are reported in Table 1. It is observed that the values are in the range of the mean literature value of 2.8, which is based on adsorption measurements reported for 23 media from seven separate studies. Interestingly, the largest measured log

Koc value is for the Hanford medium, which has the largest iron oxide content but with very little organic carbon. This again supports that composition and content of each component in the porous media contributes to PFOS adsorption.

4. Conclusion

The results reported herein for PFAS transport represent to our knowledge the first examination of the influence of nonideal sorption/desorption processes on PFAS transport in soil with a specific characterization of mass-transfer-limited elution tailing. The breakthrough curves measured for PFOS transport in two soils and the aquifer media to a lesser extent exhibited extensive elution tailing, indicating that sorption/desorption was significantly nonideal under the extant laboratory conditions. Based on the experiments and mathematical modeling, it was determined that the nonideal behavior was caused primarily by rate-limited sorption/desorption.

Standard miscible-displacement studies typically employ pore-water velocities and column lengths that are not representative of field conditions. A question of critical interest is the impact of rate-limited sorption/desorption on PFAS transport at the field scale. This issue was examined by conducting a set of simulations with the CDMR model wherein the mean pore-water velocity was decreased by a factor of 10 and the system length was increased by a factor of 10, resulting in an overall factor of 100 increase in mean hydraulic residence time. The simulations produced for parameter values representing PFOS and TCE transport in the Eustis soil are presented in Figure 11. The extent of elution tailing for PFOS is reduced but not eliminated, whereas TCE elution remains significantly rate limited. These results suggest that rate-limited sorption/desorption for PFOS may be

relevant for conditions governed by relatively short residence times, such as for example, in near-well regions of induced-gradient well fields employed for remediation projects.

Concentrations of concern for potential human-health impacts of PFOS and other PFAS are much lower than for other organic contaminants. As noted above, the U.S. EPA recently established a lifetime health advisory level of 70 ng/L for PFOS and PFOA combined for exposure via drinking water. The number of pore volumes required to reach various PFOS concentrations after the start of flushing with PFOS-free solution (i.e., elution pore volumes) can be determined from the PFOS-transport simulation presented in Figure 11. PFOS concentrations of 400, 70, 10, and 1 ng/L are attained after approximately 10, 13, 17, and 22 elution pore volumes, respectively. These are substantially larger than the approximately 5 elution pore volumes that would be required if sorption/desorption was instantaneous. It is important to keep in mind that the conditions for the simulations presented in Figure 11 represent a factor of 100 increase in hydraulic residence time, including a travel distance of 2 meters. Travel distances and associated residence times are substantially greater for many field sites, and the impact of rate-limited sorption/desorption is likely to become increasingly less significant for these greater residence times as the difference between the characteristic times of sorption/desorption and field-scale hydraulic-residence times increases. However, the results suggest that rate-limited sorption/desorption could under certain conditions increase the amount of flushing and the associated time required to reduce PFOS concentrations to levels below those associated with human-health concerns.

Acknowledgements

This research was supported by the NIEHS Superfund Research Program (grant # P42 ES04940).

References

- ALY, Y. H., LIU, C., MCINNIS, D. P., LYON, B. A., HATTON, J., MCCARTY, M., ARNOLD, W. A., PENNELL, K. D. & SIMCIK, M. F. 2018. In Situ Remediation Method for Enhanced Sorption of Perfluoro-Alkyl Substances onto Ottawa Sand. *Journal of Environmental Engineering*, 144, 9.
- ASTDR (AGENCY FOR TOXIC SUBSTANCES AND DISEASE REGISTRY) 2018. Toxicological Profile for Perfluoroalkyls.
- BRUSSEAU, M. L., YAN, N., VAN GLUBT, S., WANG, Y. K., CHEN, W., LYU, Y., DUNGAN, B., CARROLL, K. C. & HOLGUIN, F. O. 2019. Comprehensive retention model for PFAS transport in subsurface systems. *Water Research*, 148, 41-50.
- ENVIRONMENTAL PROTECTION AGENCY. 2016. Fact sheet-PFOS & PFOA. November 2017. EPA 505-F-17-001
- KEMPF, A. & BRUSSEAU, M. L. 2009. Impact of non-ideal sorption on low-concentration tailing behavior for atrazine transport in two natural porous media. *Chemosphere*, 77, 877-882.
- KEY, B. D., HOWELL, R. D. & CRIDDLE, C. S. 1997. Fluorinated organics in the biosphere. *Environmental Science & Technology*, 31, 2445-2454.
- LV, X. Y., SUN, Y. Y., JI, R., GAO, B., WU, J. C., LU, Q. S. & JIANG, H. 2018. Physicochemical factors controlling the retention and transport of perfluorooctanoic acid (PFOA) in saturated sand and limestone porous media. *Water Research*, 141, 251-258.
- LYU, Y., BRUSSEAU, M. L., CHEN, W., YAN, N., FU, X. R. & LIN, X. Y. 2018. Adsorption of PFOA at the Air-Water Interface during Transport in Unsaturated Porous Media. *Environmental Science & Technology*, 52, 7745-7753.

- MCKENZIE, E. R., SIEGRIST, R. L., MCCRAY, J. E. & HIGGINS, C. P. 2015. Effects of Chemical Oxidants on Perfluoroalkyl Acid Transport in One-Dimensional Porous Media Columns. *Environmental Science & Technology*, 49, 1681-1689.
- RUSSO, A., JOHNSON, G. R., SCHNAAR, G. & BRUSSEAU, M. L. 2010. Nonideal transport of contaminants in heterogeneous porous media: 8. Characterizing and modeling asymptotic contaminant-elution tailing for several soils and aquifer sediments. *Chemosphere*, 81, 366-371.
- SANTAMARIA, J., BRUSSEAU, M. L., ARAUJO, J., OROSZ-COGLAN, P., BLANFORD, W. J. & GERBA, C. P. 2012. Transport and Retention of *Cryptosporidium Parvum* Oocysts in Sandy Soils. *Journal of Environmental Quality*, 41, 1246-1252.
- SCHNAAR, G. & BRUSSEAU, M. L. 2014. Nonideal Transport of Contaminants in Heterogeneous Porous Media: 11. Testing the Experiment Condition Dependency of the Continuous Distribution Rate Model for Sorption-Desorption. *Water Air and Soil Pollution*, 225, 9.
- ZAREITALABAD, P., SIEMENS, J., HAMER, M. & AMELUNG, W. 2013. Perfluorooctanoic acid (PFOA) and perfluorooctanesulfonic acid (PFOS) in surface waters, sediments, soils and wastewater - A review on concentrations and distribution coefficients. *Chemosphere*, 91, 725-732.
- ZHANG, C. J., YAN, H., LI, F., HU, X. & ZHOU, Q. 2013. Sorption of short- and long-chain perfluoroalkyl surfactants on sewage sludges. *Journal of Hazardous Materials*, 260, 689-699.

Table 1. Properties of porous media. From Russo et al. (2010); Santamaria et al. (2012).

Medium	TOC (%)	Fe-oxides (mg/kg)	Mn-oxides (mg/kg)	Total-oxides (mg/kg)	Median Grain Diameter d_{50} (mm)	K_d (cm ³ /g)	Log Koc
Eustis	0.38	310	19	329	0.27	0.76	2.3
Vinton	0.1	1700	130	1830	0.26	0.54	2.7
Borden	0.03	383	70	453	0.21	0.19	2.8
AFP 44	0.06	NA	NA	NA	0.33	0.23	2.6
Hanford	0.06	14620	227	14847	0.25	0.61	3.0
Sand	0.04	14	2.5	16.5	0.35	0.15	2.6

NA = not available

Borden oxide content data from Reinhard et al., 1990.

Table 2. Constituents of synthetic groundwater.

Major cations	Concentration (mg/L)	Major anions	Concentration (mg/L)
Na⁺¹	50	NO3⁻¹	6
Ca⁺²	36	Cl⁻¹	60
Mg⁺²	25	CO3⁻²/HCO3⁻¹	133
		SO4⁻²	99

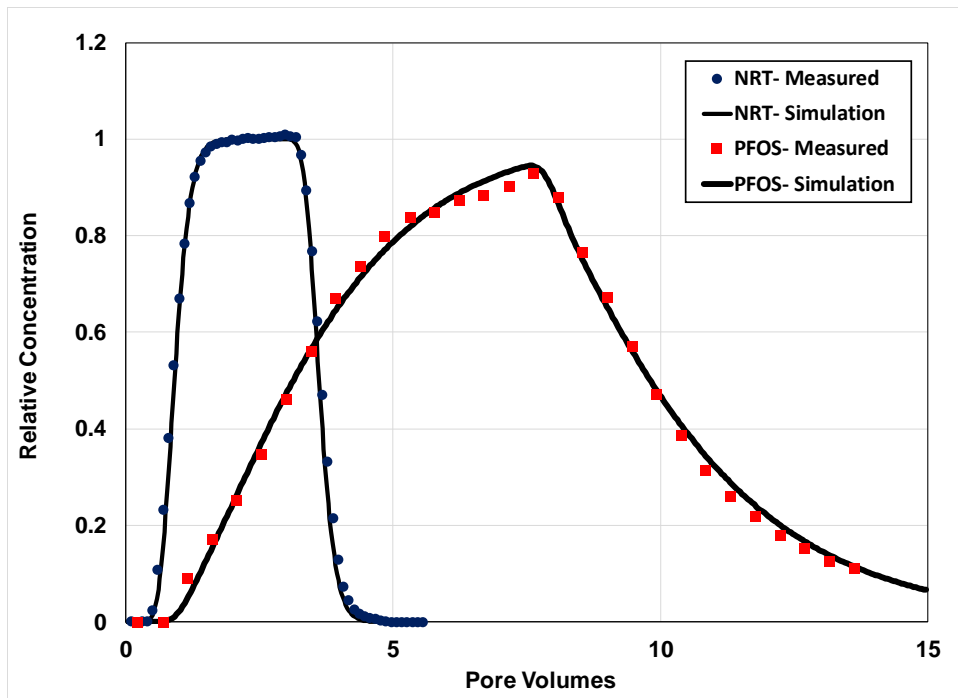


Figure 1. Measured and simulated breakthrough curves for transport of the nonreactive tracer (NRT) and PFOS in Eustis soil (Experiment 1). The PFOS simulation is produced using a two-domain model that accounts for nonlinear, rate-limited sorption/desorption ($\beta = 0.35$, $\omega = 2.5$).

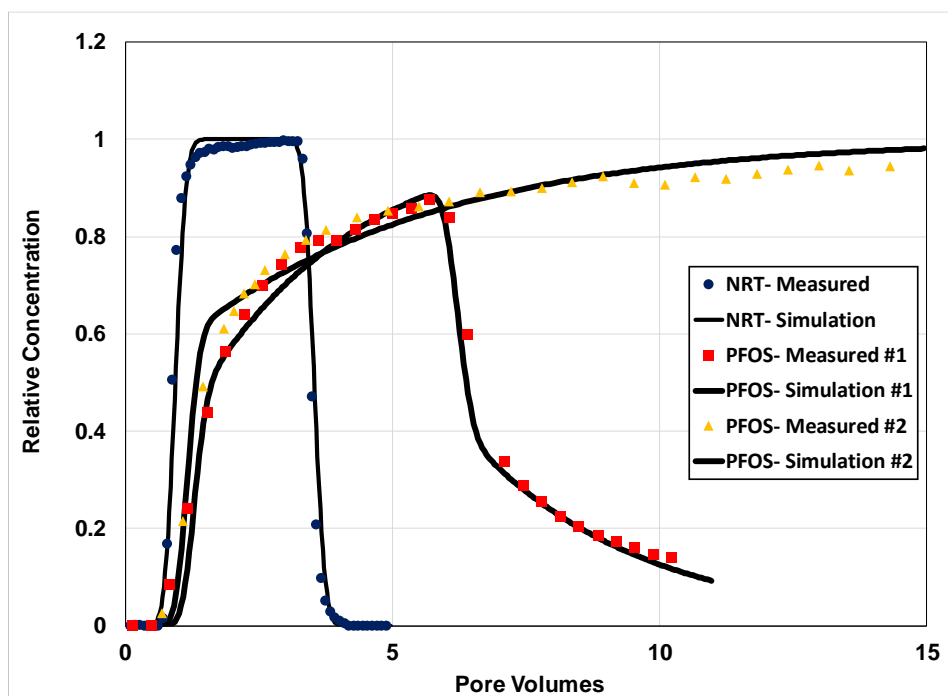


Figure 2. Measured and simulated breakthrough curves for transport of the nonreactive tracer (NRT) and PFOS in Vinton soil (Experiments 1 and 2). The PFOS simulation is produced using a two-domain model that accounts for nonlinear, rate-limited sorption/desorption (expt 1: $\beta = 0.39$, $\omega = 0.5$; expt 2: $\beta = 0.46$, $\omega = 0.74$).

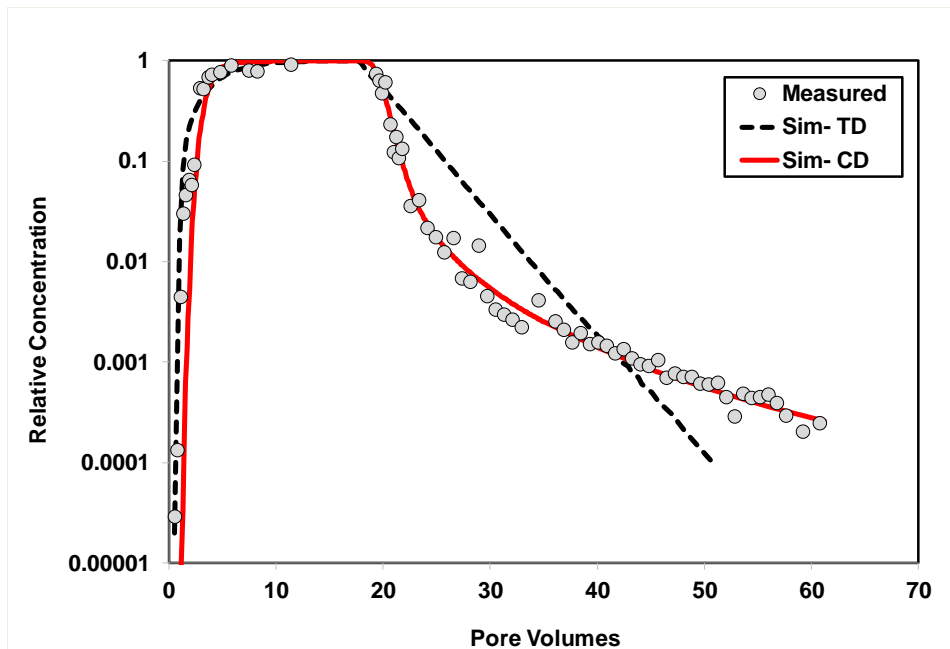


Figure 3. Measured and simulated breakthrough curves for transport of PFOS (Experiment 2) in Eustis soil. The simulations are produced using the two-domain sorption-kinetics model (TD) and the continuous-distribution multi-rate model (CD).

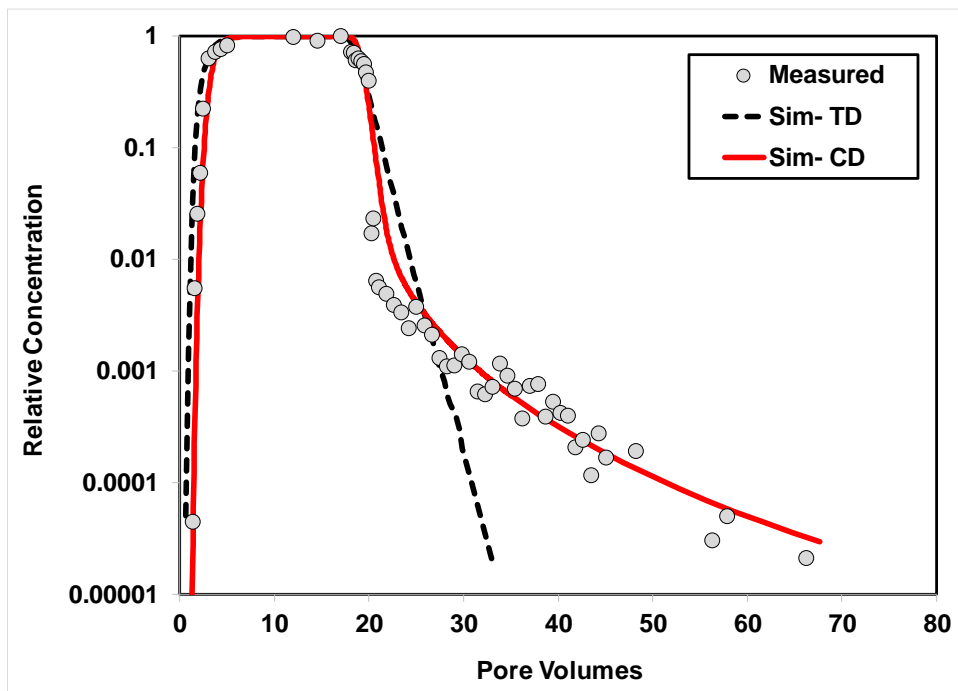


Figure 4. Measured and simulated breakthrough curves for transport of PFOS in Vinton soil (Experiment 3). The PFOS simulations are produced using the two-domain sorption-kinetics model (TD) and the continuous-distribution multi-rate model (CD).

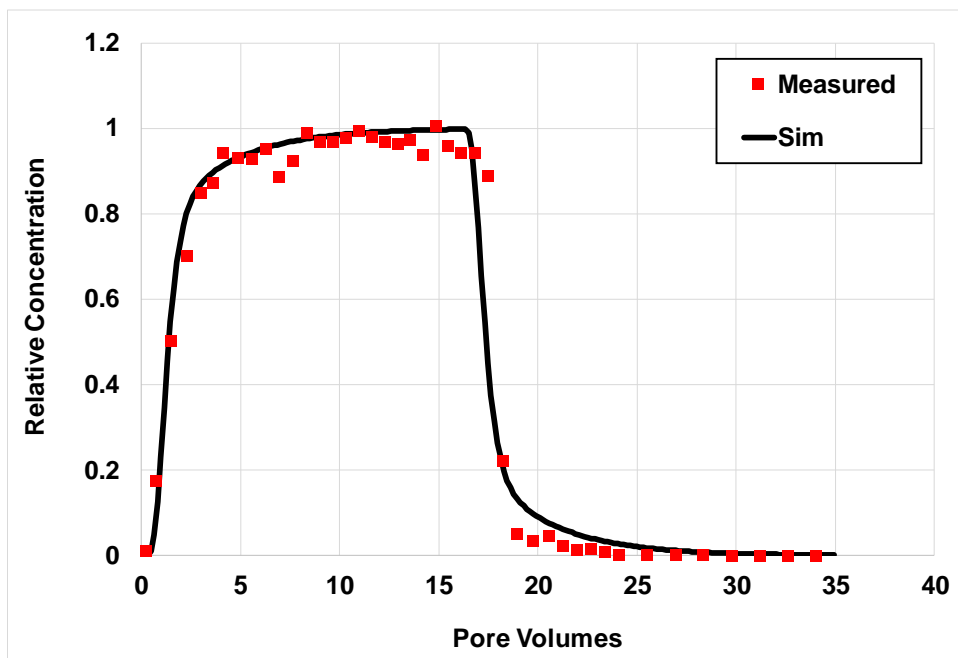


Figure 5. Measured and simulated breakthrough curves for transport of PFOS in Borden soil. The simulations are produced using the two-domain sorption-kinetics model (TD).

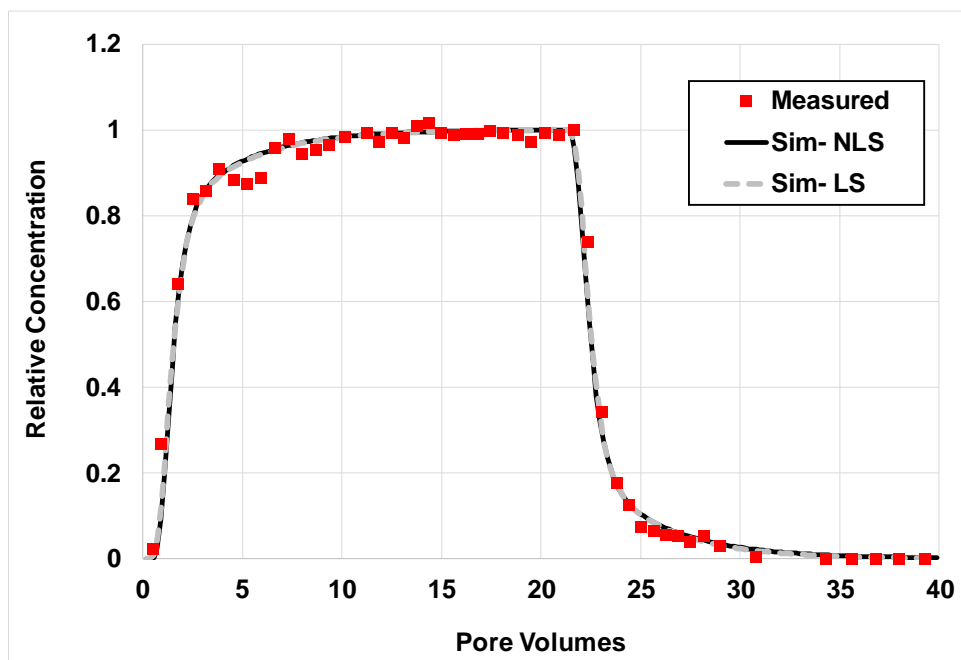


Figure 6. Measured and simulated breakthrough curves for transport of PFOS in AFP 44 soil. The simulations are produced using the two-domain sorption-kinetics model (TD), including both linear and nonlinear adsorption.

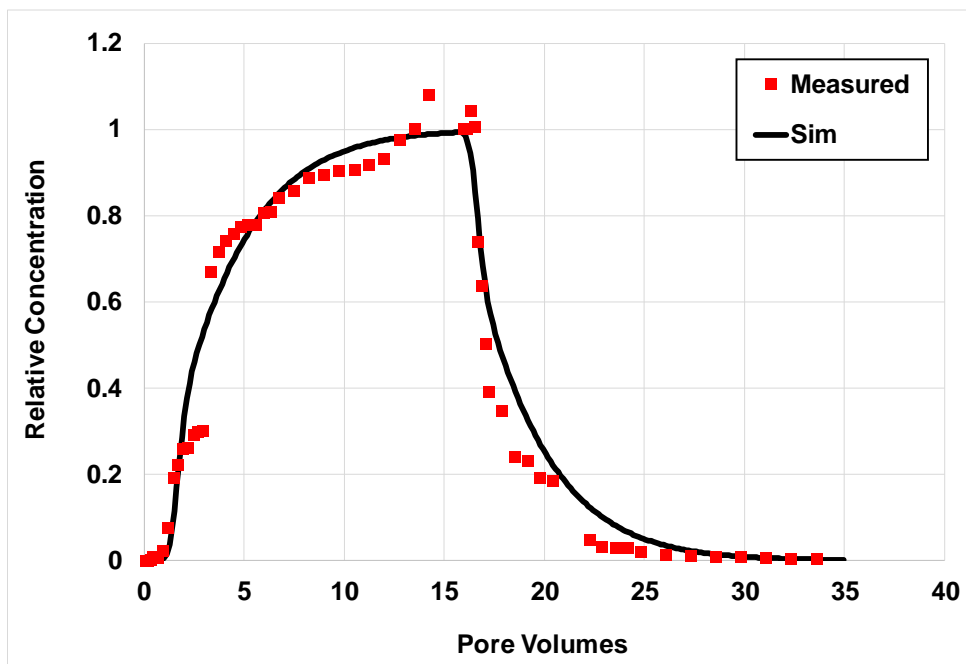


Figure 7. Measured and simulated breakthrough curves for transport of PFOS in Hanford aquifer material. The simulations are produced using the two-domain sorption-kinetics model (TD).

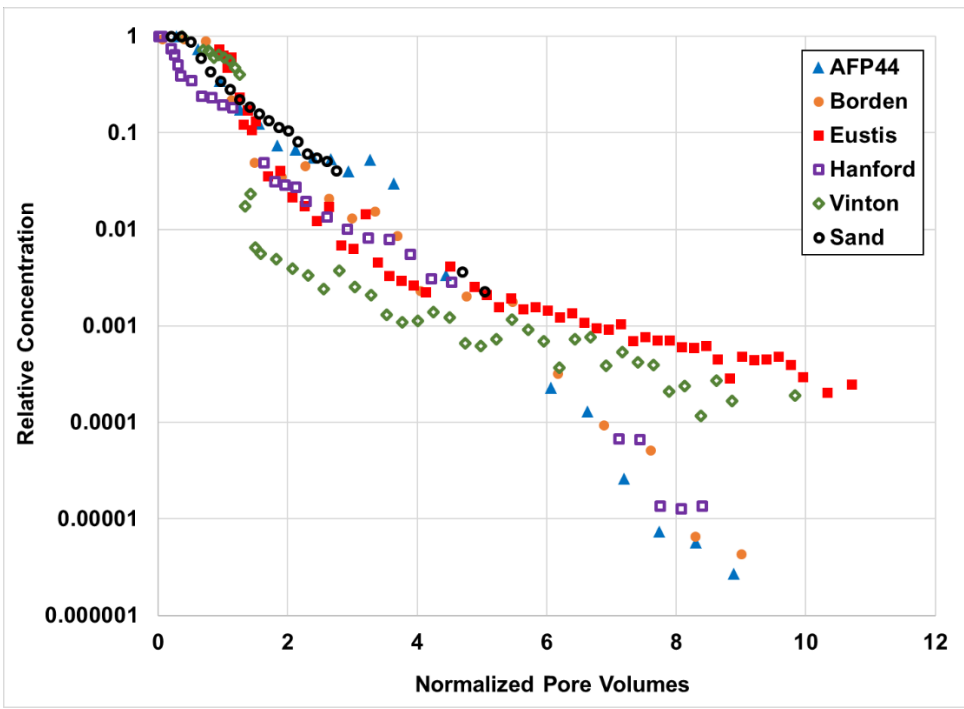


Figure 8. Normalized elution curves for PFOS transport in six porous media.

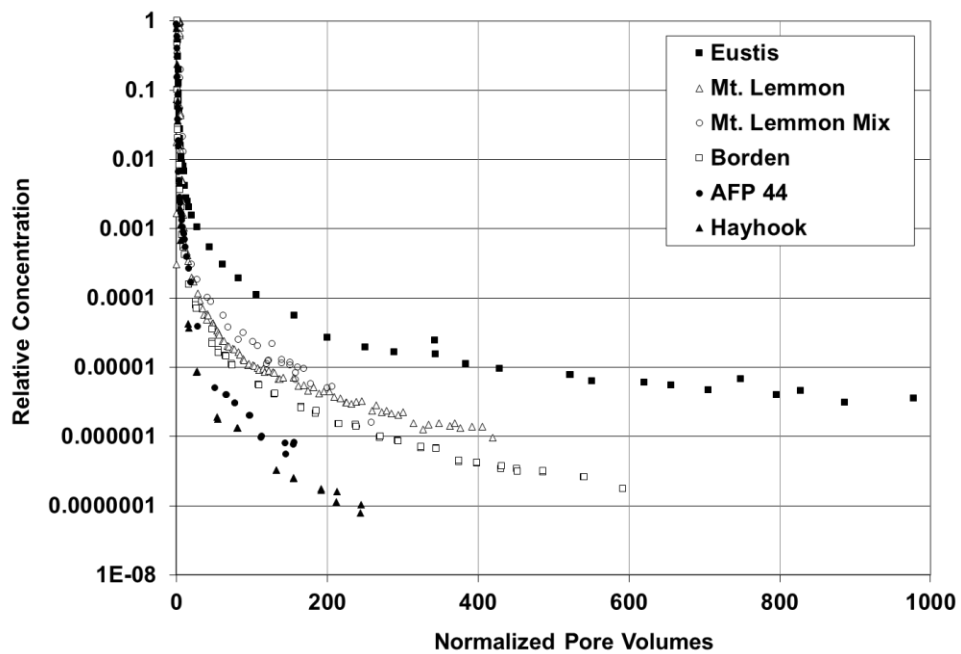


Figure 9. Normalized elution curves for TCE in various porous media. Data reported in Russo et al. (2010).

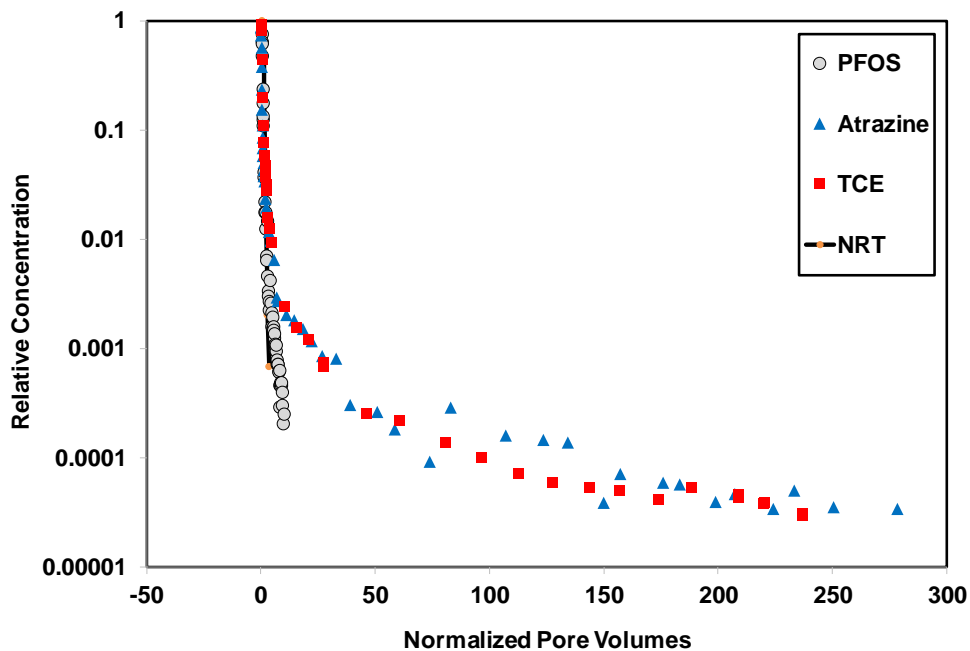


Figure 10. Normalized elution curves for PFOS, two HOCs, and a non-reactive tracer (NRT) in Eustis soil. The pore volumes are normalized by dividing by the respective retardation factors (NRT = 1, PFOS = 4.2, atrazine = 3.5, and TCE = 3). The atrazine data were reported in Kempf and Brusseau (2009) and the TCE data were reported in Schnaar and Brusseau (2014).

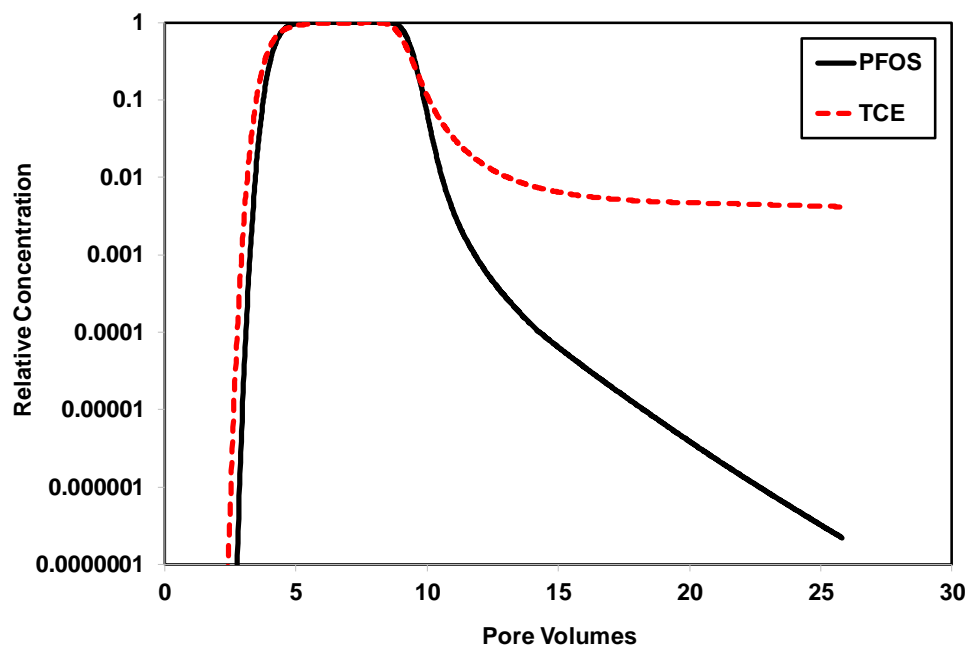


Figure 11. Simulated breakthrough curves for PFOS and TCE transport in the Eustis soil for system conditions representing a factor of 100 increase in residence time compared to the conditions used for the miscible-displacement experiments. See the main text for more information.